



저작자표시-비영리-변경금지 2.0 대한민국

이용자는 아래의 조건을 따르는 경우에 한하여 자유롭게

- 이 저작물을 복제, 배포, 전송, 전시, 공연 및 방송할 수 있습니다.

다음과 같은 조건을 따라야 합니다:



저작자표시. 귀하는 원저작자를 표시하여야 합니다.



비영리. 귀하는 이 저작물을 영리 목적으로 이용할 수 없습니다.



변경금지. 귀하는 이 저작물을 개작, 변형 또는 가공할 수 없습니다.

- 귀하는, 이 저작물의 재이용이나 배포의 경우, 이 저작물에 적용된 이용허락조건을 명확하게 나타내어야 합니다.
- 저작권자로부터 별도의 허가를 받으면 이러한 조건들은 적용되지 않습니다.

저작권법에 따른 이용자의 권리는 위의 내용에 의하여 영향을 받지 않습니다.

이것은 [이용허락규약\(Legal Code\)](#)을 이해하기 쉽게 요약한 것입니다.

[Disclaimer](#)

Master of Science

**DISTURBANCE OBSERVER-BASED CHATTERING-FREE
TERMINAL SLIDING MODE CONTROL FOR NONLINEAR
SYSTEMS SUBJECT TO MATCHED AND MISMATCHED
DISTURBANCES**

**The Graduate School
of the University of Ulsan
School of Mechanical Engineering
DUC GIAP NGUYEN**

**DISTURBANCE OBSERVER-BASED CHATTERING-FREE
TERMINAL SLIDING MODE CONTROL FOR NONLINEAR
SYSTEMS SUBJECT TO MATCHED AND MISMATCHED
DISTURBANCES**

Supervisor: Professor KYOUNG KWAN AHN

A Dissertation

Submitted to
the Graduate School of the University of Ulsan
In Partial Fulfillment of the Requirement
for the Degree of

MASTER OF SCIENCE
(Mechanical and Automotive Engineering)

by

DUC GIAP NGUYEN

School of Mechanical Engineering

University of Ulsan, Korea

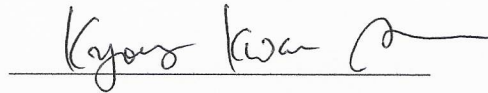
June 2021

**DISTURBANCE OBSERVER-BASED CHATTERING-
FREE TERMINAL SLIDING MODE CONTROL FOR
NONLINEAR SYSTEMS SUBJECT TO MATCHED AND
MISMATCHED DISTURBANCES**

This certifies that the dissertation of
NGUYEN DUC GIAP is approved by



Committee Chair: Prof. BYOUNG RYOUNG LEE



Committee member: Prof. KYOUNG KWAN AHN



Committee member: Prof. CHEOL KEUN HA

Department of Mechanical and Automotive Engineering

University of Ulsan, Korea

June 2021

Master of Science

**DISTURBANCE OBSERVER-BASED CHATTERING-FREE
TERMINAL SLIDING MODE CONTROL FOR
NONLINEAR SYSTEMS SUBJECT TO MATCHED AND
MISMATCHED DISTURBANCES**

**The Graduate School
of the University of Ulsan
School of Mechanical Engineering**

DUC GIAP NGUYEN

**DISTURBANCE OBSERVER-BASED CHATTERING-FREE
TERMINAL SLIDING MODE CONTROL FOR NONLINEAR
SYSTEMS SUBJECT TO MATCHED AND MISMATCHED
DISTURBANCES**

Supervisor: Professor KYOUNG KWAN AHN

A Dissertation

Submitted to
the Graduate School of the University of Ulsan
In Partial Fulfillment of the Requirement
for the Degree of

MASTER OF SCIENCE
(Mechanical and Automotive Engineering)

by

DUC GIAP NGUYEN

School of Mechanical Engineering

University of Ulsan, Korea

June 2021

Acknowledgments

I would like to express my sincere appreciation and gratitude to my advisor, Professor Kyoung Kwan Ahn for the study opportunity, his support and encouragement throughout my study at the University of Ulsan.

I would express my appreciation to my colleagues in the FPMI lab, Mr Duc Thien Tran, Mr Tri Dung Dang, Mr Hoai Vu Anh Truong, Mr Tri Cuong Do, Mr Cong Phat Vo, Mr Xuan Dinh To, Mr Cong Minh Ho, Mr Chau Duy Le, Mr Quang Tan Nguyen, Mr Hoang Vu Dao, Mr Abu Naushad Parvez, Mr M. Shahriar, Mr Hoai An Trinh, Mr Van Du Phan, Mr Duy Linh Vu, Mr Cong Hung Nguyen, Mr Yong Soo Park, Mr Thanh Ha Le, Mr Quoc Hung Hoang for their helpful discussions, great supports, inspirations and precious friendship.

Importantly, my appreciation goes towards my parents who always provide support and encouragement for me. I truly appreciate my brother and sister for their countless support.

Ulsan, Korea, June 2021

Duc Giap Nguyen

Contents

Acknowledgments.....	I
Contents	II
List of Figures	III
List of Tables	V
Nomenclature	VI
ABSTRACT.....	VII
Chapter 1 INTRODUCTION.....	1
1.1 Background.....	1
1.2 Problem statement.....	3
1.3 Research Objectives and Outline	6
Chapter 2 DISTURBANCE-OBSERVER-BASED TERMINAL SLIDING MODE CONTROL DESIGN FOR A CLASS OF SECOND-ORDER NONLINEAR SYSTEMS	9
2.1 Nonlinear Finite-time Disturbance Observer Design	9
2.2 Disturbance Observer-based Chattering-free Full-order Terminal Sliding Mode Control Design	10
Chapter 3 GENERALIZATION TO THE NTH-ORDER NONLINEAR SYSTEMS.	14
3.1 Towards the Problem of Stabilization.....	14
3.2 Towards the Problem of Tracking Control	17
Chapter 4 SIMULATIONS AND EXPERIMENTS	22
4.1 Case Study 1: Numerical Example	22
4.2 Case Study 2: Stabilizing an Electro Hydrostatic Actuator System in Simulation...29	
4.3 Case Study 3: Voltage Control for Bidirectional DC-DC Converter	39
4.4 Case study 4: Experimental Validation on an Electro Hydrostatic Actuator (EHA) System.....	50
Chapter 5 CONCLUSION AND FUTURE WORK.....	56
5.1 Summary.....	56
5.2 Future work.....	57
References.....	58

List of Figures

Figure 1. Response trajectories of state x_1 .	23
Figure 2. Response trajectories of state x_2 .	24
Figure 3. Response trajectories of control signal.	24
Figure 4. Trajectory of the mismatched disturbance.	24
Figure 5. Response trajectories of disturbance estimation error.	26
Figure 6. Sliding mode surface trajectory delivered by the proposed controller.	26
Figure 7. Effectiveness of the lowpass-filter-like approach in sliding surface (a) and control signal (b).	27
Figure 8. Influence of design parameters on observer performance.	28
Figure 9. Nominal performance preservation capability of the proposed controller.	29
Figure 10. Schematic diagram of the EHA system.	30
Figure 11. Response position trajectories in case of same (a) and different (b) control parameters.	35
Figure 12. Response velocity trajectories of EHA system.	35
Figure 13. Response nominal acceleration trajectories of the EHA system.	36
Figure 14. Response control signals of the EHA system.	36
Figure 15. Mismatched disturbance existing in the EHA system.	37
Figure 16. Mismatched disturbance estimation errors of the proposed controller.	37
Figure 17. Response chamber pressures for the DOBTSMC case.	37
Figure 18. Circuit diagram of a bidirectional DC-DC converter.	39
Figure 19. Equivalent circuit diagram of the state 1: Q_1 ON - Q_2 OFF.	40
Figure 20. Equivalent circuit diagram of state 2: Q_1 OFF - Q_2 ON.	41
Figure 21. MATLAB-Simscape modeling of the system.	44
Figure 22. Output voltage response (a) and voltage tracking error (b) of the converter.	46
Figure 23. Inductor current response of the converter.	46
Figure 24. Duty cycle response of the converter: Original (a) and Filtered (b).	47
Figure 25. Mismatched disturbance (a) and its estimation error (b).	48
Figure 26. Matched disturbance (a) and its derivative (b) existing in the system.	48
Figure 27. Photograph of the experimental apparatus.	52
Figure 28. Position tracking errors of PID and the proposed controller.	53

Figure 29. Control input trajectory of PID and the proposed control algorithm.	54
Figure 30. External force and its estimation using the proposed disturbance observer.....	54
Figure 31. Working pressures of cylinder chambers.	55

List of Tables

Table 1. Major components in the considered EHA system.....	30
Table 2. List of parameters used to model the EHA system.....	31
Table 3. Nominal Value of the EHA System Parameters.....	34
Table 4. Nominal Values of the Bidirectional Converter Parameters	45

Nomenclature

x_i	System states
f, g	Known smooth nonlinear functions
d_i	Matched or mismatched disturbances
ϕ_i	Maximum absolute value of disturbances
ρ_i	Maximum absolute value of disturbances' derivatives
s, σ	Sliding mode surfaces
α_i, c_i	Equivalent control design parameters
k_T, T, η	Switching control design parameters
u_{eq}	Equivalent control term
u_n	Switching control term
z_{ij}	Observer states
v_{ij}	Observer internal states
L_i	Lipschitz constants of disturbances
λ_{ij}, μ_{ij}	Observer design parameters

ABSTRACT

In a class of nonlinear systems that is susceptible to both matched and mismatched disturbances, the working performance can be greatly influenced and deteriorated if these disturbances are not considered in controller design. While matched disturbances enter the system in the same channel as the control input, mismatched disturbances act in a different channel and are more difficult to deal with. This work proposes a finite-time disturbance observer-based terminal sliding mode control for a class of nonlinear systems subject to both matched and mismatched disturbances.

The proposed control algorithm is first developed to stabilizing a class of second-order nonlinear systems subject to both matched and mismatched disturbances. This scheme employs a nonlinear finite-time disturbance observer to estimate mismatched disturbances fast and accurately. The result obtained from the observer is then utilized in the controller design to suppress the influence of the mismatched disturbances. To overcome the nonlinear characteristics, unmodeled dynamics, parameter uncertainties and matched disturbances, a terminal sliding mode control scheme is applied for its finite-time convergence and robustness against disturbances. The structure of a chattering-free full-order terminal sliding mode control is used to design the control algorithm to alleviate chattering and singularity phenomena in the control signal. Later in this dissertation, the proposed control algorithm is extended to the n th-order nonlinear systems. Also, besides stabilizing, the control algorithm is modified and then utilized to address the problem of tracking control. Stability analyses are provided after the mathematical formulation to support the controller design.

Four different study cases are carried out to verify the effectiveness of the proposed control algorithm. The first numerical simulation is given to assess and discuss the performance of the proposed controller theoretically. The second simulation study on controlling an electro hydrostatic actuator system partly reflects the practicality of the proposed controller. In the first two simulation studies, the proposed control algorithm is compared with a conventional terminal sliding mode control and an extended-state-observer-based sliding mode control for better performance evaluation. The third study is a task of controlling a bidirectional DC-DC converter, in which the proposed controller is used to suppress the influence of disturbances and produce a desired output voltage value. The final study is carried out in an experimental

setup, where the proposed control algorithm was implemented to solve the problem of displacement tracking control for an electro hydrostatic actuator system. PID controller is also employed in this case study for comparison. Throughout the studies, the proposed control algorithm has proved its effectiveness in stabilizing and tracking control for different systems that exhibit both matched and mismatched disturbances. However, more rigorous experiments should be conducted to validate the superiority over other control algorithms.

Chapter 1

INTRODUCTION

1.1 Background

Sliding mode control (SMC), as one of the most popular control algorithms, possesses several desirable characteristics such as design simplicity, ease of implementation and robustness to external disturbances, model uncertainties and parameter variations. Thus, SMC has been receiving a tremendous amount of attention and is widely found in diverse practical applications including robotics [1-6], electrical and mechanical systems [7-12] and aerospace engineering [13-17]. Nonetheless, the conventional SMC still exhibits several drawbacks, namely chattering, asymptotic convergence and being susceptible to mismatched disturbances.

Chattering phenomena occur in the conventional SMC owing to the use of a switching function, which leads to high oscillations in the control signal [18]. Enormous efforts have been made in the literature to attenuate this problem including boundary layer [19], second and higher-order SMC [20-22], low-pass filtering [23, 24] and disturbance observer [25]. Another problem found in the conventional SMC is that system states can only asymptotically converge to the equilibrium point. On the other hand, terminal sliding mode control (TSMC) can drive system states both to the sliding mode surface and to the equilibrium point in finite-time [26]. Although the conventional TSMC inherits the robustness characteristic from its predecessor, it still suffers from the chattering phenomenon and is prone to the singularity problem as the control signal instantly jumps to infinity. A mass of studies devoted to solving this problem, to name just a few, can be referred to [27-29]. Recently, a chattering-free full-order TSMC is developed in [30], which satisfactorily resolves both chattering and singularity problems mentioned above.

A rather less common problem that SMC faces is mismatched disturbances, which act in a different channel with the control input. Examples in which mismatched disturbances exist are MAGLEV suspension systems, permanent magnet synchronous motor systems and flight control systems [31]. Various methods that contribute to tackling this problem are integral SMC [32-34] and adaptive SMC [35-37]. However, it is well known that the integral action might produce several undesirable effects such as large overshoot and long settling time to the control system. Also, the nominal performance is normally sacrificed for robustness against

disturbances in these methods. Disturbance observer-based SMC, on the other hand, is a more promising approach to deal with mismatched disturbances [31, 38-42]. In [38], a nonlinear disturbance observer is introduced to develop a new sliding mode surface in an attempt to attenuate the mismatched disturbance. However, the mismatched disturbance considered in this work must be constant instead of time-varying, which is a very restrictive constraint as the disturbance can continuously change over time in practical applications. In other words, unless the mismatched disturbance is time-invariant, the algorithm [38] fails to stabilize the control system. Besides, the nonlinear disturbance observer utilized in [38] is proved to be exponentially stable only in case of slowly time-varying mismatched disturbances [43]. A remedy for this constant restriction on the mismatched disturbance formulation is provided in [39]. There, the proposed extended disturbance observer can estimate nonlinear and time-varying mismatched disturbances. However, the problem of being Lyapunov stable without convergence remains, thus limits the potential of the control algorithm. Another effort to stabilize nonlinear systems can be referred to [41], where mismatched disturbances are estimated and then suppressed by an extended-state-observer based sliding mode control. Both matched and mismatched disturbances are considered in this paper. Nonetheless, the estimation errors and the system state can only reach and vary in a small region around the equilibrium point, indicating that the observer and the closed-loop system are only of Lyapunov stable without convergence. Consequently, the mismatched disturbance cannot be estimated precisely, and the system state cannot be stabilized in finite time.

Motivated by previous works, to accurately estimate and eventually counter the effect of mismatched disturbances for a class of nonlinear systems, a new design of disturbance observer-based TSMC is introduced in this paper. The finite-time disturbance observer employed in this work can be easily found in the literature. There, an arbitrary-order exact robust differentiator developed in [21] forms a basis for the development of this observer, which has been employed by a large number of researchers in various applications. Some of the works are mentioned as follows. In [44], a continuous terminal sliding mode control is integrated with a finite-time disturbance observer to tackle the tracking control problem of robotic manipulators. The composite controller is introduced with finite-time convergence property in the presence of disturbances and with nominal control performance recovery ability in the absence of disturbances. Also, the control law is shown to be continuous and free from chattering. In [45], the influence of mismatched disturbances on a class of nonlinear systems is attenuated by a continuous nonsingular terminal sliding mode control based on a finite-time

disturbance observer. The property of nominal performance recovery and chattering attenuation of this control algorithm is verified in a simulation example of a Permanent magnet Synchronous Motor (PMSM). The same disturbance observer is employed in [46] to solve to problem of airgap control of a MAGnetic LEViation (MAGLEV) suspension vehicle in the presence of both matched and mismatched disturbances. There, a new dynamic sliding surface is developed by incorporating the information of the estimates of disturbances and their derivatives. Another application of this disturbance observer can be found in [31], where the authors integrate it with a nonsingular terminal sliding mode surface to control a DC-DC buck converter. Simulation and experiments on the converter have proved that the proposed control algorithm provides good disturbance rejection ability in the presence of matched and mismatched disturbances. These references have convincingly demonstrated the effectiveness of the high-order disturbance observer-based controllers in estimating and suppressing the influences of matched and mismatched disturbances in different nonlinear dynamic systems.

Major features of the proposed control algorithm include the following points. First, mismatched disturbances are rapidly estimated with great precision by a nonlinear finite-time disturbance observer. Second, a new terminal sliding mode surface developed based on the disturbance estimation results enhances the robustness against external disturbances, uncertainties and unmodeled dynamics of the control system. Third, the utilization of a chattering-free full-order terminal sliding mode surface structure in design effectively suppresses chattering and singularity phenomena in the control signal. Fourth, Lyapunov stability analysis, which is given alongside the design step, theoretically increases the reliability of the proposed control scheme. Besides, comparative simulation and experimental studies including a numerical example and the application to an Electro Hydrostatic Actuator (EHA) system and a bidirectional DC-DC converter are provided to demonstrate the performance and effectiveness of the proposed algorithm. Finally, although the control algorithm is developed for a class of nonlinear second-order systems, the obtained results can be extended to the n th-order form.

1.2 Problem statement

Consider a typical class of second-order nonlinear systems subject to both matched and mismatched disturbances as follows [41]:

$$\begin{cases} \dot{x}_1(t) = x_2(t) + d_1(t) \\ \dot{x}_2(t) = f(x, t) + g(x, t)u(t) + d_2(t) \\ y(t) = x_1(t) \end{cases} \quad (1)$$

where $x = [x_1, x_2]^T$ is the system state and assumed to be available, $f(x, t)$ and $g(x, t) \neq 0$ are two known smooth nonlinear functions, $u(t)$ is the control input, $y(t)$ is the system output, and $d_i(t)$, $i = 1, 2$ are the time-varying mismatched and matched disturbances of the system.

Assumption 1: Both mismatched and matched disturbances $d_i(t)$, $i = 1, 2$, as well as their derivatives, are bounded and satisfy:

$$|d_i(t)| \leq \phi_i, \quad |\dot{d}_i(t)| \leq \rho_i, \quad i = 1, 2 \quad (2)$$

where $\phi_i > 0$ and $\rho_i > 0$, ($i = 1, 2$) are positive constants. This assumption is reasonably realistic due to the physical limitation of machinery in practical applications.

This work aims to design a disturbance observer-based terminal sliding mode controller to drive the system state $x_1(t)$ to the origin in finite-time in the presence of matched and mismatched disturbances. From this line, where the context is sufficiently explicit, the arguments of a function might be omitted for brevity.

For the system (1), the chattering-free full-order TSMC developed in [30] is derived as below. First, a new terminal sliding mode surface is introduced with the form:

$$s = \dot{x}_2 + c_2 |x_2|^{\alpha_2} \text{sign}(x_2) + c_1 |x_1|^{\alpha_1} \text{sign}(x_1) \quad (3)$$

Then, the control law is designed accordingly as:

$$u = g^{-1}(x, t)(u_{eq} + u_n) \quad (4)$$

where u_{eq} denotes the equivalent control and u_n denotes the switching term. While u_{eq} is designed as

$$u_{eq} = -f(x, t) - c_2 |x_2|^{\alpha_2} \text{sign}(x_2) - c_1 |x_1|^{\alpha_1} \text{sign}(x_1) \quad (5)$$

u_n is defined and filtered by the following method.

$$\dot{u}_n + T u_n = v \quad (6)$$

$$v = -(\rho_2 + k_T + \eta) \text{sign}(s) \quad (7)$$

where η is a positive constant, $T \geq 0$, k_T is chosen satisfying $k_T \geq T\phi_2$, c_i and α_i ($i = 1, 2$)

are positive constants. c_i can be selected to ensure that the polynomial $p^2 + c_2 p + c_1$ is Hurwitz, and α_i can be determined to satisfy [30, 47]:

$$\begin{cases} \alpha_1 = \frac{\alpha_2}{2 - \alpha_2} \\ \alpha_2 = \alpha, \alpha \in (1 - \varepsilon, 1), \varepsilon \in (0, 1) \end{cases} \quad (8)$$

By substituting the system (1) and the control law (4) and (5) into the sliding surface (3), one can obtain:

$$\begin{aligned} s &= \dot{x}_2 + c_2 |x_2|^{\alpha_2} \text{sign}(x_2) + c_1 |x_1|^{\alpha_1} \text{sign}(x_1) \\ &= f(x, t) + g(x, t)u + d_2(t) + c_2 |x_2|^{\alpha_2} \text{sign}(x_2) + c_1 |x_1|^{\alpha_1} \text{sign}(x_1) \\ &= d_2(t) + u_n \end{aligned} \quad (9)$$

Consider a candidate Lyapunov function of the form: $V(s) = \frac{1}{2} s^2$. It is proved in [48] that

$|u_n(t)| \leq \phi_2$ and this statement is depicted here for better understanding. Initially, $u_n(t=0) = 0$ is taken, i.e. $u_n(0) \in [-\phi_2, \phi_2]$. Then, u_n is proved that it cannot leave $[-\phi_2, \phi_2]$. Recall that $|d_2| \leq \phi_2$, $|\dot{d}_2| \leq \rho_2$ in (2) and $k_T \geq T\phi_2$ in the first line after (7). Denote $\beta = \rho_2 + k_T + \eta$. Due to $s = u_n + d_2$ in (9), (6) can be rewritten as

$$\dot{u}_n + Tu_n = -\beta \text{sign}(s) = -\beta \text{sign}(u_n + d_2) \quad (10)$$

If $u_n > \phi_2$, then $u_n + T\phi_2 > 0$, $\text{sign}(u_n + d_2) = \text{sign}(u_n) = 1$. It can be obtained from (10) that:

$$\dot{u}_n = -Tu_n - \beta < 0$$

In the same way, if $u_n < -\phi_2$, then $\text{sign}(u_n + d_2) = \text{sign}(u_n) = -1$. It can be obtained from (10) that:

$$\dot{u}_n = -Tu_n + \beta > 0$$

Thus, the inequality $u_n \dot{u}_n < 0$ holds outside of $[-\phi_2, \phi_2]$, and u_n cannot leave $[-\phi_2, \phi_2]$, i.e. $|u_n| \leq \phi_2$ is kept for any $t \geq 0$.

Due to $|u_n| \leq \phi_2$, which is proved in the above step, accordingly, $|\dot{d}_2(t) + Tu_n(t)| \leq \rho_2 + T\phi_2$ are kept for any $t \geq 0$. Differentiate the Lyapunov function $V(s)$, it follows that:

$$\begin{aligned}
s\dot{s} &= s(\dot{d}_2 + \dot{u}_n) \\
&= s(\dot{d}_2 + (\dot{u}_n + Tu_n) - Tu_n) \\
&= s(\dot{d}_2 + v - Tu_n) \\
&\leq \left(|\dot{d}_2 - Tu_n| - (\rho_2 + k_T + \eta) \right) |s| \\
&= \left(|\dot{d}_2 - Tu_n| - (\rho_2 + T\phi_2) - (k_T - T\phi_2) - \eta \right) |s| \\
&\leq -\eta |s|
\end{aligned} \tag{11}$$

The inequality (11) indicates that the system states will reach the sliding surface $s = 0$ in finite time. Once the desired sliding mode $s = 0$ is established, the dynamics of the system can be expressed as

$$\begin{cases} \dot{x}_1 = x_2 + d_1(t) \\ \dot{x}_2 = -c_2 |x_2|^{\alpha_2} \text{sign}(x_2) - c_1 |x_1|^{\alpha_1} \text{sign}(x_1) \end{cases} \tag{12}$$

In case there are no mismatched disturbances, (12) will become:

$$\begin{cases} \dot{x}_1 = x_2 \\ \dot{x}_2 = -c_2 |x_2|^{\alpha_2} \text{sign}(x_2) - c_1 |x_1|^{\alpha_1} \text{sign}(x_1) \end{cases} \tag{13}$$

From (13), if c_i and α_i , $i = 1, 2$ are chosen as below (7) and as in (8), respectively, then the system states will converge to the equilibrium in finite time [47, 49]. However, in case mismatched disturbances exist, based on the equation set (12), one can obtain the below relationship:

$$\ddot{x}_1 + c_2 |\dot{x}_1 - d_1|^{\alpha_2} \text{sign}(\dot{x}_1 - d_1) + c_1 |x_1|^{\alpha_1} \text{sign}(x_1) = \dot{d}_1 \tag{14}$$

It is clear from the above equation that despite the control effort, the mismatched disturbance still exists in the system dynamics. Thus, the resulted system state is strongly affected by the mismatched disturbance. In other words, even though the system state can be attracted to the sliding surface in finite-time, it cannot converge to the equilibrium point owing to the presence of the time-varying mismatched disturbance. This is the reason why the chattering-free TSMC developed in [30] can cope with matched disturbances yet fail to overcome the influence of mismatched disturbances.

1.3 Research Objectives and Outline

The research objectives are listed as follows.

- Design a disturbance-observer-based terminal sliding mode control for the task of stabilizing a class of second-order nonlinear systems subject to both matched and mismatched disturbances.
- Extend the obtained results to stabilize a class of n th-order nonlinear systems.
- Modify the proposed control algorithm to solve the problem of tracking control for a class of n th-order nonlinear systems.
- Verify the effectiveness of the proposed algorithm via numerical simulations and experimental setup.

The dissertation consists of five chapters, which are organized as follows.

Chapter 1 gives a detailed introduction to the research. One of the main concerns is the existence of mismatched disturbances in a class of nonlinear systems. The other concern is the problem that a conventional chattering-free full-order terminal sliding mode control is faced with as dealing with mismatched disturbances in such type of nonlinear systems. This draws out the motivation for this research.

In Chapter 2, the solution to the problem is delivered in two steps. Step 1 introduces the nonlinear finite-time disturbance observer to accurately estimate the mismatched disturbances existing in the system. Step 2 presents the design of a disturbance-observer-based terminal sliding mode control, which utilizes the disturbance estimation result to suppress the influence of the mismatched disturbances. This chapter also introduces the chattering-free full-order structure that alleviates the problem of chattering and singularity in conventional terminal sliding mode control. The mathematical formulation is followed by a stability analysis to support the design.

In Chapter 3, the designed control algorithm for second-order systems is extended for the n th-order systems including the generalization of the system, the disturbance observer and the terminal sliding mode controller. This chapter continues extending the proposed control algorithm to address the problem of tracking control.

In Chapter 4, four different case studies are introduced to verify the effectiveness of the proposed control algorithm. The first numerical simulation is given to help assess and discuss the performance of the proposed control algorithm theoretically. The second simulation on stabilizing an electro hydrostatic actuator partly reflects the practicality of the proposed controller. The third study on voltage control a bidirectional DC-DC converter proves that the proposed control algorithm can be applied for different kinds of system. This study also introduces a new control-oriented modeling approach for a bidirectional DC-DC converter so

that it is more convenient to apply nonlinear control algorithms. The fourth study provides experimental validation for the proposed control algorithm as it is employed to control the displacement of an electro hydrostatic actuator system.

Chapter 5 provides conclusions and future work.

Chapter 2

DISTURBANCE-OBSERVER-BASED TERMINAL SLIDING MODE CONTROL DESIGN FOR A CLASS OF SECOND-ORDER NONLINEAR SYSTEMS

In this section, a new chattering-free full-order terminal sliding mode control powered by a nonlinear disturbance observer is proposed for the system (1). First, the disturbance observer is employed to estimate the mismatched disturbance followed by a finite-time convergence analysis. After that, a new terminal sliding surface and a control law are developed to ensure that the system state will converge to the origin in finite time.

2.1 Nonlinear Finite-time Disturbance Observer Design

The objective of this section is to employ a finite-time disturbance observer to estimate the time-varying mismatched disturbance existing in (1). Based on the research on globally convergent differentiators in [50], a nonlinear disturbance observer is designed as follows.

$$\begin{cases} \dot{z}_1 = v_1 + x_2 \\ v_1 = -\lambda_1 L^{1/3} |z_1 - x_1|^{2/3} \text{sign}(z_1 - x_1) - \mu_1 (z_1 - x_1) + z_2 \\ \dot{z}_2 = v_2 \\ v_2 = -\lambda_2 L^{1/2} |z_2 - v_1|^{1/2} \text{sign}(z_2 - v_1) - \mu_2 (z_2 - v_1) + z_3 \\ \dot{z}_3 = -\lambda_3 L \text{sign}(z_3 - v_2) - \mu_3 (z_3 - v_2) \end{cases} \quad (15)$$

where $z_1 = \hat{x}_1$, $z_2 = \hat{d}_1$, $z_3 = \dot{\hat{d}}_1$, and $L > 0$, $\lambda_i, \mu_i > 0$ ($i = 1, 2, 3$).

Assumption 2: The time-varying mismatched disturbance $d_1(t)$ is assumed to be second-order differentiable and has a Lipschitz constant L .

Theorem 1: Given that the disturbance observer is designed as (15), if the design parameters are properly selected, the following results are achieved in finite-time.

$$z_1 = x_1, \quad z_2 = d_1, \quad z_3 = \dot{d}_1 \quad (16)$$

Proof. For the disturbance observer (15), define the estimation errors as follows.

$$\varepsilon_1 = \frac{z_1 - x_1}{L}, \quad \varepsilon_2 = \frac{z_2 - d_1}{L}, \quad \varepsilon_3 = \frac{z_3 - \dot{d}_1}{L} \quad (17)$$

By taking the derivative of ε_1 , ε_2 and ε_3 , one can obtain the observer error dynamics:

$$\begin{cases} \dot{\varepsilon}_1 = -\lambda_1 |\varepsilon_1|^{2/3} \text{sign}(\varepsilon_1) - \mu_1 \varepsilon_1 + \varepsilon_2 \\ \dot{\varepsilon}_2 = -\lambda_2 |\varepsilon_2 - \dot{\varepsilon}_1|^{1/2} \text{sign}(\varepsilon_2 - \dot{\varepsilon}_1) - \mu_2 (\varepsilon_2 - \dot{\varepsilon}_1) + \varepsilon_3 \\ \dot{\varepsilon}_3 = -\lambda_3 \text{sign}(\varepsilon_3 - \dot{\varepsilon}_2) - \mu_3 (\varepsilon_3 - \dot{\varepsilon}_2) - \frac{1}{L} \ddot{d}_1 \end{cases} \quad (18)$$

Then, according to **Theorem 3.1, Lemma B.1** and their proofs in [50], the estimation errors (18) will converge to zero in finite-time, indicating that the nonlinear disturbance observer can accurately estimate the system state $x_1(t)$, the time-varying mismatched disturbance $d_1(t)$ and its derivative $\dot{d}_1(t)$. This completes the proof of *Theorem 1*.

Remark 1: Viewers are strongly encouraged to read the works [21, 50, 51] and the references therein to further understand the rigorous stability analysis of the disturbance observer as well as how to properly choose its design parameters. It is noted in these above references that the observer design parameters, $\{\lambda_i, \mu_i\} (i=1,2,3)$, are chosen recursively in such a way that $\{\lambda_i, \mu_i\}$ provide for the convergence of the observer with the Lipschitz constant L indicated in *Assumption 2*. It is also mentioned by the authors that these parameters can be easily changed since it is not very sensitive to their values. The tradeoff is as follows: generally, the greater the parameters, the faster convergence of the disturbance observer yet higher sensitivity to input noises and the sampling step and larger peaking phenomenon in the control signal if the initial values of the system states and those of the observer states are different. Thus, in the case of different initial values, a tradeoff could be made to ensure fast convergence yet acceptable peaking phenomenon.

2.2 Disturbance Observer-based Chattering-free Full-order Terminal Sliding Mode Control Design

In this section, based on the disturbance estimation, a new sliding surface is proposed, then accordingly a new control law is designed to drive the system state to the equilibrium point in finite time. Motivated by the work on chattering-free full-order SMC in [30], this work can also be considered as an extension to the control strategies developed in [41] and [30].

A new disturbance observer (DOB)-based terminal sliding mode surface for the system (1) is proposed as:

$$\sigma = \dot{x}_2 + c_2 |x_2 + z_2|^{\alpha_2} \text{sign}(x_2 + z_2) + c_1 |x_1|^{\alpha_1} \text{sign}(x_1) + z_3 \quad (19)$$

where $z_2 = \hat{d}_1$, $z_3 = \hat{d}_1$ obtained from the disturbance observer, c_i and α_i ($i=1,2$) are positive constants. c_i are chosen to guarantee that the polynomial $p^2 + c_2 p + c_1$ is Hurwitz, and α_i are determined as same as in (8).

Theorem 2: Given the sliding surface (19), if the control law is developed as

$$u = g^{-1}(x,t)(u_{eq} + u_n) \quad (20)$$

with the equivalent control

$$u_{eq} = -f(x,t) - c_2 |x_2 + z_2|^{\alpha_2} \text{sign}(x_2 + z_2) - c_1 |x_1|^{\alpha_1} \text{sign}(x_1) - z_3 \quad (21)$$

and the switching term is filtered for chattering attenuation as

$$\dot{u}_n + T u_n = v \quad (22)$$

$$v = -(\rho_2 + k_T + \eta) \text{sign}(\sigma) \quad (23)$$

where T , k_T , η are defined as same as below (7), then the system (1) will reach the sliding mode surface $\sigma = 0$ in finite-time, and the system state $x_1(t)$ will converge to the origin in finite-time also.

Proof. By substituting the expression of $\dot{x}_2(t)$ in (1) and the control law (20), (21) into the sliding surface (19), one can derive the following equality:

$$\begin{aligned} \sigma &= \dot{x}_2 + c_2 |x_2 + z_2|^{\alpha_2} \text{sign}(x_2 + z_2) + c_1 |x_1|^{\alpha_1} \text{sign}(x_1) + z_3 \\ &= [f(x,t) + g(x,t)u + d_2(t)] + c_2 |x_2 + z_2|^{\alpha_2} \text{sign}(x_2 + z_2) + c_1 |x_1|^{\alpha_1} \text{sign}(x_1) + z_3 \\ &= d_2(t) + u_n \end{aligned} \quad (24)$$

Consider a candidate Lyapunov function as $V(\sigma) = \frac{1}{2} \sigma^2$. Differentiating the Lyapunov function $V(\sigma)$ and following the same procedure in (11) yields:

$$\begin{aligned} \dot{V}(\sigma) &= \sigma \dot{\sigma} \\ &= \sigma [\dot{d}_2(t) + \dot{u}_n] \\ &\leq -\eta |\sigma| \end{aligned} \quad (25)$$

which implies that the system will arrive at the sliding surface $\sigma = 0$ in finite time. Once the desired sliding mode occurs, combining system (1) and sliding surface (19), one can obtain:

$$\begin{cases} \dot{x}_1 = x_2 + d_1 \\ \dot{x}_2 = -c_2 |x_2 + z_2|^{\alpha_2} \text{sign}(x_2 + z_2) - c_1 |x_1|^{\alpha_1} \text{sign}(x_1) - z_3 \end{cases} \quad (26)$$

From the equation set (26), the following relationship can be established:

$$\begin{aligned} \ddot{x}_1 &= \dot{x}_2 + \dot{d}_1 \\ &= \left[-c_2 |x_2 + z_2|^{\alpha_2} \text{sign}(x_2 + z_2) - c_1 |x_1|^{\alpha_1} \text{sign}(x_1) - z_3 \right] + \dot{d}_1 \\ &= -c_2 |(\dot{x}_1 - d_1) + z_2|^{\alpha_2} \text{sign}((\dot{x}_1 - d_1) + z_2) - c_1 |x_1|^{\alpha_1} \text{sign}(x_1) - z_3 + \dot{d}_1 \\ &= -c_2 |\dot{x}_1 + (z_2 - d_1)|^{\alpha_2} \text{sign}(\dot{x}_1 + (z_2 - d_1)) - c_1 |x_1|^{\alpha_1} \text{sign}(x_1) - (z_3 - \dot{d}_1) \end{aligned} \quad (27)$$

According to **Theorem 1**, $z_2 = d_1$ and $z_3 = \dot{d}_1$ are achieved in finite time by the disturbance observer. Thus, the equation (27) becomes:

$$\ddot{x}_1 = -c_2 |\dot{x}_1|^{\alpha_2} \text{sign}(\dot{x}_1) - c_1 |x_1|^{\alpha_1} \text{sign}(x_1) \quad (28)$$

Let $w_1 = x_1$, $w_2 = \dot{x}_1$, the dynamic equation (28) can be transformed into

$$\begin{cases} \dot{w}_1 = w_2 \\ \dot{w}_2 = u \end{cases} \quad (29)$$

where $u = -c_2 |w_2|^{\alpha_2} \text{sign}(w_2) - c_1 |w_1|^{\alpha_1} \text{sign}(w_1)$, and c_i, α_i ($i=1,2$) are designed as same as below equation (19) and equation (8). Then, according to Proposition 8.1 and its proof in [47], it can be concluded that the origin is a globally finite-time-stable equilibrium for the system (29), indicating that the state $x_1(t)$ of the system (1) will eventually converge to zero in finite time. This completes the proof for **Theorem 2**.

Remark 2: As stated in [30], the control signal (22) acts in the same manner as a low-pass filter, where $\omega = T$ can be interpreted as the bandwidth of the filter. The non-smooth switching function u_n is therefore smoothed to prevent the chattering phenomena from happening if the design parameters are properly chosen. Also, being a full-order sliding mode surface, it allows deriving the corresponding control law without differentiating the term $c_i |*|^{\alpha_i} \text{sign}(*)$, thus avoiding singularity.

Remark 3: It should be mentioned that the sliding surface (19) includes the ‘acceleration’ signal $\dot{x}_2(t)$, which can be obtained through differentiating the ‘velocity’ signal $x_2(t)$. Nonetheless, this action is sensitive to noises and thus can degrade system performance. Notice that the proposed control law only utilizes the sign of the sliding surface σ instead of its value.

Based on this observation, the same idea suggested in [30] is depicted here to avoid the use of the ‘acceleration’ signal. Thus, $\text{sign}(\sigma)$ can be alternatively determined as follows.

$$\text{sign}(\sigma) = \text{sign}(h(t) - h(t - \tau)) \quad (30)$$

where $h(t)$ is defined as:

$$\begin{aligned} h(t) &= \int_0^t \sigma(t) dt \\ &= x_2 + \int_0^t \left(c_2 |x_2 + z_2|^{\alpha_2} \text{sign}(x_2 + z_2) + c_1 |x_1|^{\alpha_1} \text{sign}(x_1) + z_3 \right) dt \end{aligned} \quad (31)$$

and τ is chosen to be the fundamental sampling time.

Alternatively, the nonlinear disturbance observer structure can be applied again to meet this need and is presented below.

$$\begin{cases} \dot{z}_4 = v_4 + x_3 \\ v_4 = -\lambda_4 L_2^{1/3} |z_4 - x_2|^{2/3} \text{sign}(z_4 - x_2) - \mu_4 (z_4 - x_2) + z_5 \\ \dot{z}_5 = v_5 \\ v_5 = -\lambda_5 L_2^{1/2} |z_5 - v_4|^{1/2} \text{sign}(z_5 - v_4) - \mu_5 (z_5 - v_4) + z_6 \\ \dot{z}_6 = -\lambda_6 L_2 \text{sign}(z_6 - v_5) - \mu_6 (z_6 - v_5) \end{cases} \quad (32)$$

where $x_3 = f(x, t) + g(x, t)u$, $z_4 = \hat{x}_2$, $z_5 = \hat{d}_2$, $z_6 = \hat{d}_2$. Since the disturbance observer is proved to be finite-time convergent, after a transient period, $\dot{z}_4 = \dot{\hat{x}}_2$ can be regarded as the ‘acceleration’ signal. Besides, the matched disturbance $d_2(t)$ can be accurately estimated for further use such as reducing the switching gain in the control signal (23), thus decreasing the chance chattering phenomena will occur. However, the use of another disturbance observer will increase the computational burden, which might represent a disadvantage in practical applications.

Remark 4: As the mismatched disturbance is absent from the control system, if the initial values of the observer states are selected as $z_1(t_0) = x_1(t_0)$, $z_2(t_0) = z_3(t_0) = 0$ then it is derived from the observer formulation and observer error dynamics that $\varepsilon_1(t) = \varepsilon_2(t) = \varepsilon_3(t) = 0$ and $v_1(t) = v_2(t) = 0$. In this case, the sliding surface (19) and the control law (20) will reduced to those of the conventional TSMC. This indicates the nominal control performance preservation capability of the proposed controller.

Chapter 3

GENERALIZATION TO THE NTH-ORDER NONLINEAR SYSTEMS.

3.1 Towards the Problem of Stabilization

Consider a class of nonlinear nth-order systems of the form:

$$\begin{cases} \dot{x}_i = x_{i+1} + d_i(t), & i = 1, 2, \dots, n-1 \\ \dot{x}_n = f(x, t) + g(x, t)u + d_n(t) \end{cases} \quad (33)$$

where $x_i (i=1, 2, \dots, n)$ are the system states and assumed to be available, $f(x, t)$ and $g(x, t) \neq 0$ are two known smooth nonlinear functions, u is the control input, $d_i (i=1, 2, \dots, n-1)$ and d_n are respectively the mismatched disturbances and matched disturbance of the system. Similar to *Assumption 1*, it is assumed that the disturbances and their derivatives are bounded.

$$|d_i(t)| \leq \phi_i, \quad |\dot{d}_i(t)| \leq \rho_i, \quad i = 1, 2, \dots, n \quad (34)$$

The major objective in this section is to design a control algorithm such that the system state $x_1(t)$ will converge to the equilibrium in finite time.

To accurately estimate the mismatched disturbances existing in the system, an nth-order disturbance observer can be developed as follows.

$$\begin{cases} \dot{z}_{1i} = v_{1i} + x_{i+1} = \varphi_{1i}(z_{1i} - x_i) + z_{2i} + x_{i+1} \\ \dot{z}_{2i} = v_{2i} = \varphi_{2i}(z_{2i} - v_{1i}) + z_{3i} \\ \dots \\ \dot{z}_{(n+1)i} = \varphi_{(n+1)i}(z_{(n+1)i} - v_{ni}) \end{cases} \quad (i = 1, 2, \dots, n-1) \quad (35)$$

where φ_{ji} are the nonlinear functions of the form:

$$\varphi_{ji}(s) = -\lambda_{ji} L_i^{1/(n-j+2)} |s|^{(n-j+1)/(n-j+2)} \text{sign}(s) - \mu_{ji}(s), \quad (j = 1, 2, \dots, n+1) \quad (36)$$

and $z_{1i} = \hat{x}_i$, $z_{2i} = \hat{d}_i$, $z_{3i} = \hat{\dot{d}}_i$, \dots , $z_{(n+1)i} = d_i^{(n-1)}$, $L_i > 0$, $\lambda_{ji}, \mu_{ji} > 0$, $j = 1, 2, \dots, n+1$, $i = 1, 2, \dots, n-1$.

Then, a chattering-free full-order TSMC for n th-order systems can be developed based on the disturbance observer as follows.

$$\sigma = \dot{x}_n + \sum_{k=2}^n \left(c_k |\psi_k|^{\alpha_k} \text{sign}(\psi_k) \right) + c_1 |x_1|^{\alpha_1} \text{sign}(x_1) + \chi_z \quad (37)$$

where $\psi_k = x_k + z_{k1} + z_{(k-1)2} + \dots + z_{2(k-1)}$, $\chi_z = z_{3(n-1)} + z_{4(n-2)} \dots + z_{(n+1)1} \cdot c_k$ and α_k are positive constants such that the polynomial $p^n + \sum_{k=2}^n (c_k p^{k-1}) + c_1$ is Hurwitz and the following equation set is satisfied [30, 47]:

$$\begin{cases} \alpha_1 = \alpha, & n = 1 \\ \alpha_{k-1} = \frac{\alpha_k \alpha_{k+1}}{2\alpha_{k+1} - \alpha_k}, & k = 2, \dots, n \quad \forall n \geq 2 \end{cases} \quad (38)$$

where $\alpha_{n+1} = 1$, $\alpha_n = \alpha$, $\alpha \in (1 - \varepsilon, 1)$, $\varepsilon \in (0, 1)$.

Theorem 3: Given the surface (37), if the control law is developed as

$$u = g^{-1}(x, t)(u_{eq} + u_n) \quad (39)$$

where u_{eq} denotes the equivalent control and is defined as

$$u_{eq} = -f(x, t) - \sum_{k=2}^n \left(c_k |\psi_k|^{\alpha_k} \text{sign}(\psi_k) \right) - c_1 |x_1|^{\alpha_1} \text{sign}(x_1) - \chi_z \quad (40)$$

and u_n denotes the switching term and is defined and filtered as

$$\begin{cases} \dot{u}_n + T u_n = v \\ v = -(\rho_n + k_T + \eta) \text{sign}(\sigma) \end{cases} \quad (41)$$

where $T \geq 0$ and k_T are chosen to satisfy $k_T \geq (T\phi_n)$, η is a positive constant, then the system (33) will reach the surface $\sigma = 0$ in finite time, and the system state $x_1(t)$ will also converge to the equilibrium in finite time.

Proof. Substituting the system (33) and the control law from (40) to (41) into the sliding surface (37) yields:

$$\begin{aligned} \sigma &= \dot{x}_n + \sum_{k=2}^n \left(c_k |\psi_k|^{\alpha_k} \text{sign}(\psi_k) \right) + c_1 |x_1|^{\alpha_1} \text{sign}(x_1) + \chi_z \\ &= (f + g u + d_n) + \sum_{k=2}^n \left(c_k |\psi_k|^{\alpha_k} \text{sign}(\psi_k) \right) + c_1 |x_1|^{\alpha_1} \text{sign}(x_1) + \chi_z \\ &= d_n + u_n \end{aligned} \quad (42)$$

Consider a candidate Lyapunov function $V(\sigma) = \sigma^2/2$. Differentiating this Lyapunov function and following the same procedure in (11) yields:

$$\begin{aligned}
\dot{V}(\sigma) &= \sigma \dot{\sigma} \\
&= \sigma \left[\dot{d}_n(t) + \dot{i}_n \right] \\
&\leq -\eta |\sigma|
\end{aligned} \tag{43}$$

This implies that the system states will arrive at the sliding surface $\sigma = 0$ in finite time. Once the sliding mode occurs, one can combine the system dynamics (33) and sliding surface (37) to obtain:

$$\begin{cases} \dot{x}_i = x_{i+1} + d_i, & i = 1, 2, \dots, n-1 \\ \dot{x}_n = -\sum_{k=2}^n \left(c_k |\psi_k|^{\alpha_k} \text{sign}(\psi_k) \right) - c_1 |x_1|^{\alpha_1} \text{sign}(x_1) - \chi_z \end{cases} \tag{44}$$

Based on the above equation set, the following relationship can be established:

$$x_1^{(n)} = -\sum_{k=2}^n \left(c_k |\psi_k|^{\alpha_k} \text{sign}(\psi_k) \right) - c_1 |x_1|^{\alpha_1} \text{sign}(x_1) - \chi_z + d_1^{(n-1)} + d_2^{(n-2)} + \dots + \ddot{d}_{n-2} + \dot{d}_{n-1} \tag{45}$$

where:

$$\begin{aligned}
& -\sum_{k=2}^n \left(c_k |\psi_k|^{\alpha_k} \text{sign}(\psi_k) \right) - c_1 |x_1|^{\alpha_1} \text{sign}(x_1) \\
&= -c_n \left| x_n + z_{n1} + \dots + z_{2(n-1)} \right|^{\alpha_n} \text{sign} \left(x_n + z_{n1} + \dots + z_{2(n-1)} \right) \\
&\quad - c_{n-1} \left| x_{n-1} + z_{(n-1)1} + \dots + z_{2(n-2)} \right|^{\alpha_{n-1}} \text{sign} \left(x_{n-1} + z_{(n-1)1} + \dots + z_{2(n-2)} \right) \\
&\quad \dots \\
&\quad - c_1 |x_1|^{\alpha_1} \text{sign}(x_1) \\
&= -c_n \left| x_1 - d_1^{(n-1)} - \dots - d_{n-1} + z_{n1} + \dots + z_{2(n-1)} \right|^{\alpha_n} \text{sign} \left(x_1 - d_1^{(n-1)} - \dots - d_{n-1} + z_{n1} + \dots + z_{2(n-1)} \right) \\
&\quad - c_{n-1} \left| x_1 - d_1^{(n-2)} - \dots - d_{n-2} + z_{(n-1)1} + \dots + z_{2(n-2)} \right|^{\alpha_{n-1}} \text{sign} \left(x_1 - d_1^{(n-2)} - \dots - d_{n-2} + z_{(n-1)1} + \dots + z_{2(n-2)} \right) \\
&\quad \dots \\
&\quad - c_1 |x_1|^{\alpha_1} \text{sign}(x_1)
\end{aligned}$$

and

$$\begin{aligned}
& -\chi_z + d_1^{(n-1)} + d_2^{(n-2)} + \dots + \ddot{d}_{n-2} + \dot{d}_{n-1} \\
&= -z_{3(n-1)} - z_{4(n-2)} - \dots - z_{n2} - z_{(n+1)1} + d_1^{(n-1)} + d_2^{(n-2)} + \dots + \ddot{d}_{n-2} + \dot{d}_{n-1} \\
&= \left(\dot{d}_{n-1} - z_{3(n-1)} \right) + \left(\ddot{d}_{n-2} - z_{4(n-2)} \right) - \dots + \left(d_2^{(n-2)} - z_{n2} \right) + \left(d_1^{(n-1)} - z_{(n+1)1} \right)
\end{aligned}$$

Applying **Theorem 1**, the disturbance observer developed in the previous section ensures that

$z_{1i} = x_i$, $z_{2i} = d_i$, $z_{3i} = \dot{d}_i$, ..., $z_{(n+1)i} = \overset{(n-1)}{d}_i$, $i = 1, 2, \dots, n-1$ happen in finite time. Thus, Eq.

(45) becomes:

$$x_1^{(n)} = -c_n \left| x_1 \right|^{\alpha_n} \text{sign} \left(x_1 \right) - c_{n-1} \left| x_1 \right|^{\alpha_{n-1}} \text{sign} \left(x_1 \right) - \dots - c_1 \left| x_1 \right|^{\alpha_1} \text{sign} \left(x_1 \right) \quad (46)$$

Let $w_1 = x_1$, $w_2 = \dot{x}_1$, ..., $w_{n-1} = \overset{(n-2)}{x}_1$, $w_n = \overset{(n-1)}{x}_1$, the dynamic equation (46) can be transformed into:

$$\begin{cases} \dot{w}_1 = w_2 \\ \dots \\ \dot{w}_{n-1} = w_n \\ \dot{w}_n = u \end{cases} \quad (47)$$

where $u = -c_n \left| w_n \right|^{\alpha_n} \text{sign} \left(w_n \right) - c_{n-1} \left| w_{n-1} \right|^{\alpha_{n-1}} \text{sign} \left(w_{n-1} \right) - \dots - c_1 \left| w_1 \right|^{\alpha_1} \text{sign} \left(w_1 \right)$, and c_i , α_i ($i = 1, 2, \dots, n$) are designed as same as below (37) and as (38), respectively. Then, according to Proposition 8.1 and its proof in [47], it can be concluded that the origin is a globally finite-time stable equilibrium for the system (47), indicating that the system state $x_1(t)$ will eventually converge to zero infinite time. This completes the proof for **Theorem 3**.

3.2 Towards the Problem of Tracking Control

Reconsider the class of nonlinear nth-order systems of the form:

$$\begin{cases} \dot{x}_i = x_{i+1} + d_i(t), & i = 1, 2, \dots, n-1 \\ \dot{x}_n = f(x, t) + g(x, t)u + d_n(t) \end{cases} \quad (48)$$

where x_i ($i = 1, 2, \dots, n$) are the system states and assumed to be available, $f(x, t)$ and $g(x, t) \neq 0$ are two known smooth nonlinear functions, u is the control input, d_i ($i = 1, 2, \dots, n-1$) and d_n are respectively the mismatched disturbances and matched disturbance of the system. Similar to **Assumption 1**, it is assumed that the disturbances and their derivatives are bounded.

$$\left| d_i(t) \right| \leq \phi_i, \quad \left| \dot{d}_i(t) \right| \leq \rho_i, \quad i = 1, 2, \dots, n \quad (49)$$

The primary objective of the algorithm is to ensure that the system state $x_1(t)$ tracks a reference signal $r(t)$ accurately and quickly. Thus, by establishing tracking errors as

$$\begin{cases} e_i = x_i - r^{(i-1)}, & i = 1, 2, \dots, n-1 \\ e_n = x_n - r^{(n)} \end{cases} \quad (50)$$

one can obtain the following error dynamics:

$$\begin{cases} \dot{e}_i = e_{i+1} + d_i, & i = 1, 2, \dots, n-1 \\ \dot{e}_n = f(x, t) + g(x, t)u + d_n - r^{(n)} \end{cases} \quad (51)$$

Next, a chattering-free full-order TSMC based on disturbance observer is developed as follows. First, the n th-order finite-time disturbance observer developed in the previous section is restated here for clearer illustration.

$$\begin{cases} \dot{z}_{1i} = v_{1i} + x_{i+1} = \varphi_{1i}(z_{1i} - x_i) + z_{2i} + x_{i+1} \\ \dot{z}_{2i} = v_{2i} = \varphi_{2i}(z_{2i} - v_{1i}) + z_{3i} \\ \dots \\ \dot{z}_{(n+1)i} = \varphi_{(n+1)i}(z_{(n+1)i} - v_{ni}) \end{cases} \quad (i = 1, 2, \dots, n-1) \quad (52)$$

where φ_{ji} are the functions of the following form:

$$\varphi_{ji}(s) = -\lambda_{ji} L_i^{1/(n-j+2)} |s|^{(n-j+1)/(n-j+2)} \text{sign}(s) - \mu_{ji}(s), \quad (j = 1, 2, \dots, n+1) \quad (53)$$

and $z_{1i} = \hat{x}_i$, $z_{2i} = \hat{d}_i$, $z_{3i} = \hat{d}_i$, \dots , $z_{(n+1)i} = d_i^{(n-1)}$, $L_i > 0$, $\lambda_{ji}, \mu_{ji} > 0$, $j = 1, 2, \dots, n+1$, $i = 1, 2, \dots, n-1$.

Then a chattering-free full-order terminal sliding mode surface can be designed as

$$\sigma = \dot{e}_n + \sum_{k=2}^n (c_k |\psi_k|^{\alpha_k} \text{sign}(\psi_k)) + c_1 |e_1|^{\alpha_1} \text{sign}(e_1) + \chi_z \quad (54)$$

where $\psi_k = e_k + z_{k1} + z_{(k-1)2} + \dots + z_{2(k-1)}$, $\chi_z = z_{3(n-1)} + z_{4(n-2)} + \dots + z_{(n+1)1}$, c_k and α_k are positive constants such that the polynomial $p^n + \sum_{k=2}^n (c_k p^{k-1}) + c_1$ is Hurwitz and the following set of equations is satisfied [30, 47]:

$$\begin{cases} \alpha_1 = \alpha, & n = 1 \\ \alpha_{k-1} = \frac{\alpha_k \alpha_{k+1}}{2\alpha_{k+1} - \alpha_k}, & k = 2, \dots, n \quad \forall n \geq 2 \end{cases} \quad (55)$$

where $\alpha_{n+1} = 1$, $\alpha_n = \alpha$, $\alpha \in (1 - \varepsilon, 1)$, $\varepsilon \in (0, 1)$.

Theorem 4: Given the sliding surface (54), if the control law is developed as

$$u = g^{-1}(x, t)(u_{eq} + u_n) \quad (56)$$

with the equivalent control u_{eq} is defined as

$$u_{eq} = -f(x, t) + r - \sum_{k=2}^n \left(c_k |\psi_k|^{\alpha_k} \text{sign}(\psi_k) \right) - c_1 |e_1|^{\alpha_1} \text{sign}(e_1) - \chi_z \quad (57)$$

and the switching term u_n is defined and filtered for chattering attenuation as

$$\begin{cases} \dot{u}_n + Tu_n = v \\ v = -(\rho_n + k_T + \eta) \text{sign}(\sigma) \end{cases} \quad (58)$$

where $T \geq 0$ and k_T are chosen to satisfy $k_T \geq (T\phi_n)$, η is a positive constant, then the system (48) will reach the surface $\sigma = 0$ in finite-time, and the state error $e_1(t)$ will converge to the origin in finite-time. This also indicates that the system state $x_1(t)$ will accurately track the reference $r(t)$.

Proof. By substituting the error dynamics (51) and the control law from (56) to (57) into the sliding surface (54), one can derive the following equality:

$$\begin{aligned} \sigma &= \dot{e}_n + \sum_{k=2}^n \left(c_k |\psi_k|^{\alpha_k} \text{sign}(\psi_k) \right) + c_1 |e_1|^{\alpha_1} \text{sign}(e_1) + \chi_z \\ &= \left(f + gu + d_n - r \right) + \sum_{k=2}^n \left(c_k |\psi_k|^{\alpha_k} \text{sign}(\psi_k) \right) + c_1 |e_1|^{\alpha_1} \text{sign}(e_1) + \chi_z \\ &= d_n + u_n \end{aligned} \quad (59)$$

Now consider a candidate Lyapunov function $V(\sigma) = \sigma^2/2$, differentiate this Lyapunov function, and follow the same procedure in (11) yields:

$$\begin{aligned} \dot{V}(\sigma) &= \sigma \dot{\sigma} \\ &= \sigma \left[\dot{d}_n(t) + \dot{u}_n \right] \\ &\leq -\eta |\sigma| \end{aligned} \quad (60)$$

which implies that the system will arrive at the sliding surface $\sigma = 0$ in finite time. Once the desired sliding mode occurs, combining the error dynamics (51) and sliding surface (54) yields:

$$\begin{cases} \dot{e}_i = e_{i+1} + d_i, & i = 1, 2, \dots, n-1 \\ \dot{e}_n = -\sum_{k=2}^n \left(c_k |\psi_k|^{\alpha_k} \text{sign}(\psi_k) \right) - c_1 |e_1|^{\alpha_1} \text{sign}(e_1) - \chi_z \end{cases} \quad (61)$$

From the above equation set, the following relationship can be established:

$$e_1^{(n)} = -\sum_{k=2}^n \left(c_k |\psi_k|^{\alpha_k} \text{sign}(\psi_k) \right) - c_1 |e_1|^{\alpha_1} \text{sign}(e_1) - \chi_z + d_1^{(n-1)} + d_2^{(n-2)} + \dots + \ddot{d}_{n-2} + \dot{d}_{n-1} \quad (62)$$

where

$$\begin{aligned} & -\sum_{k=2}^n \left(c_k |\psi_k|^{\alpha_k} \text{sign}(\psi_k) \right) - c_1 |e_1|^{\alpha_1} \text{sign}(e_1) \\ &= -c_n \left| e_n + z_{n1} + \dots + z_{2(n-1)} \right|^{\alpha_n} \text{sign} \left(e_n + z_{n1} + \dots + z_{2(n-1)} \right) \\ & \quad - c_{n-1} \left| e_{n-1} + z_{(n-1)1} + \dots + z_{2(n-2)} \right|^{\alpha_{n-1}} \text{sign} \left(e_{n-1} + z_{(n-1)1} + \dots + z_{2(n-2)} \right) \\ & \quad \dots \\ & \quad - c_1 |e_1|^{\alpha_1} \text{sign}(e_1) \\ &= -c_n \left| e_1 - d_1^{(n-1)} - \dots - d_{n-1}^{(n-2)} + z_{n1} + \dots + z_{2(n-1)} \right|^{\alpha_n} \text{sign} \left(e_1 - d_1^{(n-1)} - \dots - d_{n-1}^{(n-2)} + z_{n1} + \dots + z_{2(n-1)} \right) \\ & \quad - c_{n-1} \left| e_1 - d_1^{(n-2)} - \dots - d_{n-2}^{(n-3)} + z_{(n-1)1} + \dots + z_{2(n-2)} \right|^{\alpha_{n-1}} \text{sign} \left(e_1 - d_1^{(n-2)} - \dots - d_{n-2}^{(n-3)} + z_{(n-1)1} + \dots + z_{2(n-2)} \right) \\ & \quad \dots \\ & \quad - c_1 |e_1|^{\alpha_1} \text{sign}(e_1) \end{aligned}$$

and

$$\begin{aligned} & -\chi_z + d_1^{(n-1)} + d_2^{(n-2)} + \dots + \ddot{d}_{n-2} + \dot{d}_{n-1} \\ &= -z_{3(n-1)} - z_{4(n-2)} - \dots - z_{n2} - z_{(n+1)1} + d_1^{(n-1)} + d_2^{(n-2)} + \dots + \ddot{d}_{n-2} + \dot{d}_{n-1} \\ &= \left(\dot{d}_{n-1} - z_{3(n-1)} \right) + \left(\ddot{d}_{n-2} - z_{4(n-2)} \right) - \dots + \left(d_2^{(n-2)} - z_{n2} \right) + \left(d_1^{(n-1)} - z_{(n+1)1} \right) \end{aligned}$$

Whereas, following *Theorem 1*, the disturbance observer developed in the previous section

ensures that $z_{1i} = x_i$, $z_{2i} = d_i$, $z_{3i} = \dot{d}_i$, \dots , $z_{(n+1)i} = d_i^{(n-1)}$, $i=1,2,\dots,n-1$ occur in finite time.

Thus, Eq. (62) now becomes:

$$e_1^{(n)} = -c_n \left| e_1 \right|^{\alpha_n} \text{sign} \left(e_1 \right) - c_{n-1} \left| e_1 \right|^{\alpha_{n-1}} \text{sign} \left(e_1 \right) - \dots - c_1 |e_1|^{\alpha_1} \text{sign}(e_1) \quad (63)$$

Let $w_1 = e_1$, $w_2 = \dot{e}_1$, \dots , $w_{n-1} = e_1^{(n-1)}$, $w_n = e_1^{(n)}$, the dynamic equation (63) can be transformed into:

$$\begin{cases} \dot{w}_1 = w_2 \\ \dots \\ \dot{w}_{n-1} = w_n \\ \dot{w}_n = u \end{cases} \quad (64)$$

where $u = -c_n |w_{n-1}|^{\alpha_n} \text{sign}(w_{n-1}) - c_{n-1} |w_{n-2}|^{\alpha_{n-1}} \text{sign}(w_{n-2}) - \dots - c_1 |w_1|^{\alpha_1} \text{sign}(w_1)$, and c_i, α_i ($i = 1, 2, \dots, n$) are designed as same as below (54) and as (55), respectively. Then, according to Proposition 8.1 and its proof in [47], it can be concluded that the origin is a globally finite-time stable equilibrium for the system (64), indicating that the state error $e_1(t)$ will eventually converge to zero in finite time. This completes the proof for **Theorem 4**.

Chapter 4

SIMULATIONS AND EXPERIMENTS

In this section, three simulation studies and a brief experiment are provided to verify the effectiveness of the control algorithm. Whilst a numerical example is given to assess and discuss the performance of the proposed controller theoretically, the task of controlling an electro hydrostatic actuator system and a bidirectional DC-DC converter partly reflects the practicality of the suggested control algorithm. These simulations are conducted in the MATLAB-Simulink environment, wherein the fixed-step ODE4 (Runge-Kutta) is chosen to be the solver. The sampling time is determined separately for each case study, and other settings remain as default.

4.1 Case Study 1: Numerical Example

To demonstrate the effectiveness of the proposed control algorithm, the succeeding nonlinear second-order system, which is subject to time-varying mismatched and matched disturbances, is considered for simulation.

$$\begin{cases} \dot{x}_1 = x_2 + d_1(t) \\ \dot{x}_2 = -2x_1 - x_2 + e^{x_1} + u + d_2(t) \end{cases} \quad (65)$$

Here, the initial system state is selected as $x = [1, -1]^T$. The mismatched and matched disturbances are defined as $d_1(t) = 1 + 0.3 \cos(2t) - \sin(t)$ and $d_2(t) = \sin(2t)$, respectively. The mismatched disturbance is selected different from the reference [41] in terms that as time increases and the system state $x_1(t)$ reaches its steady-state value, the mismatched disturbance is still time-varying in a much larger bounded region instead of gradually converging to a constant as in reference [41]. This is an important factor in proving the superiority of the proposed control algorithm over other strategies being considered and will be illustrated by simulation results.

For comparison purpose, the chattering-free full-order TSMC approach [30], denoted by TSMC, the extended-state-observer-based chattering free SMC [41], denoted by ESOSMC, and the proposed control algorithm, denoted as DOBTSMC, are employed. It should be noted

that both the DOBTSMC and the ESOSMC stem from the TSMC. Hence, an analogy is drawn here to demonstrate the superiority of the proposed algorithm.

Briefly, the ESOSMC proposed in [41] is constructed of a nonlinear extended-state-observer (ESO) and an ESO-based SMC. The ESO is designed based on the hyperbolic tangent function of the form:

$$\begin{cases} \dot{Z}_1 = Z_2 - a_1(Z_1 - x_1) + x_2 \\ \dot{Z}_2 = -a_2 \tanh(b(Z_1 - x_1)) \end{cases} \quad (66)$$

where $Z_1 = \hat{x}_1$, $Z_2 = \hat{d}_1$, $\tanh(*) = (e^* - e^{-*}) / (e^* + e^{-*})$, $a_i > 0$, $i = 1, 2$, $b > 0$. The new sliding mode surface integrated with the ESO is developed as:

$$s = \dot{x}_2 + c_2(x_2 + Z_2) + c_1x_1 + \dot{Z}_2 \quad (67)$$

where c_i , $i = 1, 2$ are chosen in the same manner as in previous sections.

The design control parameters are specifically selected to be the same for all control algorithms as $c_1 = 6$, $c_2 = 5$, $T = 0.1$, $(\rho_2 + k_T + \eta) = 10$. Apart from that, for the TSMC and the DOBTSMC, follow (8), α_i ($i = 1, 2$) are designed as $\alpha_1 = 3/7$, $\alpha_2 = 3/5$. For the mismatched disturbance observers, ESO parameters are selected as $a_1 = 50$, $a_2 = 35$ and $b = 50$; and DOB parameters are chosen as $L = 2$, $\lambda_1 = 6$, $\lambda_2 = 11$, $\lambda_3 = 6$, $\mu_1 = 18$, $\mu_2 = 6$, $\mu_3 = 1$.

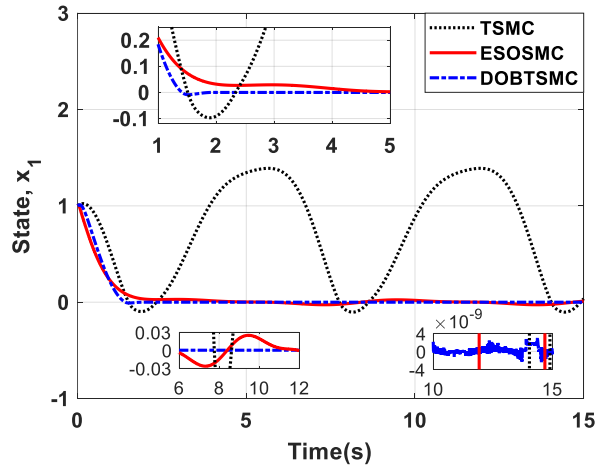


Figure 1. Response trajectories of state x_1 .

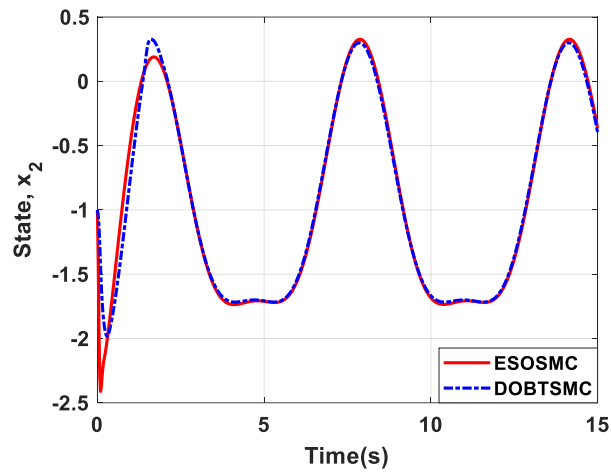


Figure 2. Response trajectories of state x_2 .

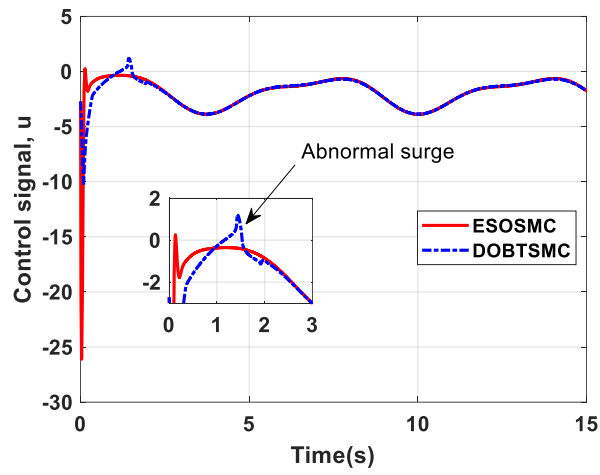


Figure 3. Response trajectories of control signal.

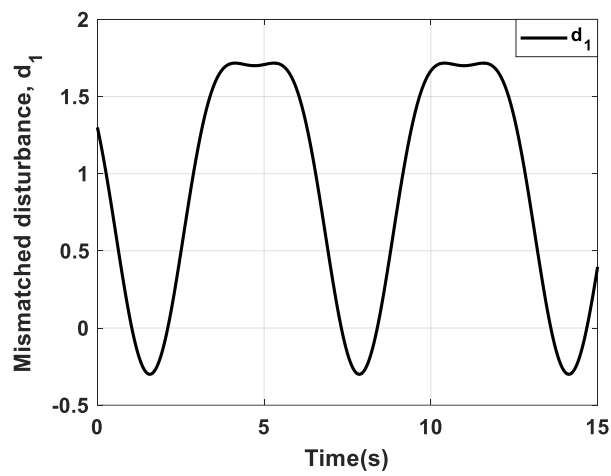


Figure 4. Trajectory of the mismatched disturbance.

The system state $x_1(t)$ delivered by all control algorithms is shown in Figure 1. It demonstrates conclusively that the TSMC fails to stabilize the system state $x_1(t)$, which is predicted by theoretical analysis in the problem statement section. Therefore, the TSMC signals are suppressed in the succeeding figures for better visualization of the other two algorithms. Also, it is evident from Figure 1 that the response state $x_1(t)$ controlled by the ESOSMC is only able to reach and then vary in a small-bounded region of $[-0.03, 0.03]$ around the equilibrium without converging to it. On the other hand, faster and finite-time convergence is seen for the DOBTSMC with the accuracy is around $4e-9$. This result proves the superior property of the proposed algorithm over the ESOSMC method.

It can be interpreted from the system (65) that to stabilize the system state $x_1(t)$ to the equilibrium point for the cases of TSMC and DOBTSMC or at least to the vicinity of the equilibrium point for the case of ESOSMC, the following inequality must be fulfilled:

$$|\dot{x}_1| = |x_2 + d_1| \leq \delta \quad (68)$$

where δ is a sufficiently small positive number and can represent the performance indicator for evaluation. Inequality (68) indicates that for the sake of stability, $x_2(t)$ must counteract the time-varying effect caused by the mismatched disturbance $d_1(t)$. Consequently, $x_2(t)$ and $d_1(t)$ should be symmetric about the time axis. This statement can be observed by comparing the trajectory shape of the state $x_2(t)$ in Figure 2 to that of the mismatched disturbance $d_1(t)$ in Figure 4. It also explains why the system state $x_1(t)$ but not $x_2(t)$ converges to the equilibrium.

The illustration of control signals generated by the ESOSMC and the DOBTSMC are shown in Figure 3. Both the ESOSMC and the DOBTSMC algorithm exhibit a smooth control signal without chattering effects. However, a much greater peaking effect at the beginning is seen for the ESOSMC compared with the DOBTSMC. Reducing observer gains of the ESOSMC can be a solution to alleviate the severity of this phenomenon. Nevertheless, at the same time, this action will produce a larger disturbance estimation error, thus deteriorate the overall performance. In contrast, the DOBTSMC exhibits satisfactory performance without a serious peaking phenomenon in the control signal. This further proves that the proposed algorithm is more effective in dealing with time-varying mismatched disturbances than the ESOSMC. Closely looking at Figure 3, an abnormal surge exists in the control signal of the proposed

algorithm during the transient period before the system state $x_1(t)$ reaches its steady-state value. This phenomenon occurs because of the use of an absolute value function in the controller design. Since the absolute value function is continuous but of piecewise linearity at zero, whenever the argument of the absolute function changes its sign, nonlinearity will happen, and the corresponding surge will appear.

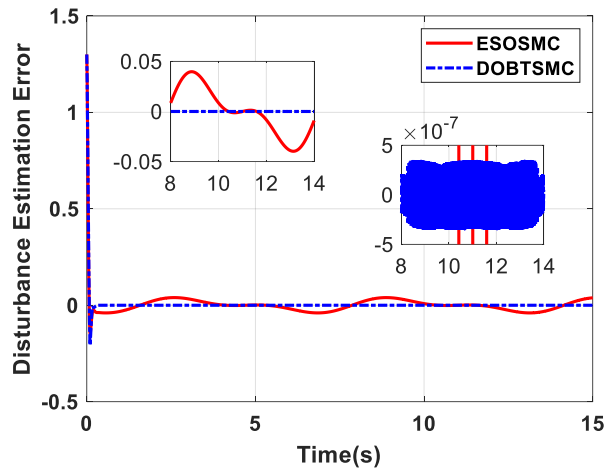


Figure 5. Response trajectories of disturbance estimation error.

Figure 4 depicts the mismatched disturbance trajectory, which is nonlinear and time-varying throughout the simulation period. Whereas, the mismatched disturbance estimation errors of both ESOSMC and DOBTSMC depicted in Figure 5 shows an agreement with the statement discussed on the system state $x_1(t)$ in Figure 1. While finite-time convergence is seen for the DOBTSMC, the ESOSMC can only reach the Lyapunov stable state. This clearly indicates that the proposed control algorithm outperforms the ESOSMC in disturbance estimation and attenuation.

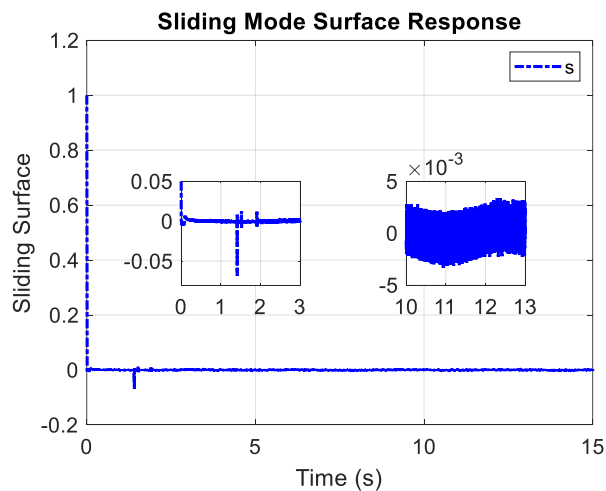


Figure 6. Sliding mode surface trajectory delivered by the proposed controller.

Figure 6 depicts the trajectory of the sliding surface produced by the proposed control algorithm. Except for some abnormal surges occurring in the transition period due to the piecewise linearity of the absolute value functions used in the controller design, the sliding mode surface appears to converge to the equilibrium almost right after start, which contributes to the fast response of the controller.

To demonstrate the effectiveness of the low-pass-filter like approach in alleviating the chattering phenomenon, a comparison is drawn out as follows. Two switching control term is utilized for comparison, including the original switching control term u_{n1} :

$$u_{n1} = -\beta \text{sign}(s) \quad (69)$$

and the filtered switching control term u_{n2} :

$$\begin{cases} \dot{u}_{n2} + Tu_{n2} = v \\ v = -\beta \text{sign}(s) \end{cases} \quad (70)$$

where s is the sliding mode surface, $T = 0.1$ is the bandwidth of the filter, and $\beta = 10$ is the design switching control parameter. Other aspects of the simulation study are kept to be the same. The comparison result is presented in Figure 7 below.

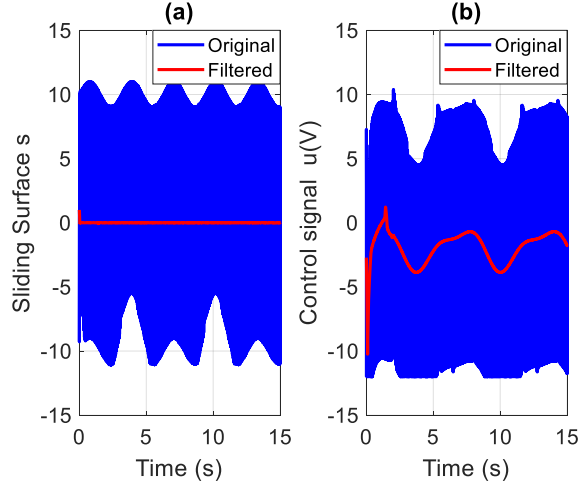


Figure 7. Effectiveness of the lowpass-filter-like approach in sliding surface (a) and control signal (b).

It is clear from Figure 1 that the lowpass-filter-like approach (70) has significantly suppressed the chattering phenomenon in both the control signal and the sliding surface. The control command signal is smooth except for some abnormal surges appearing in the transition period, which is caused by the piecewise linearity of the absolute value functions utilized in the controller design.

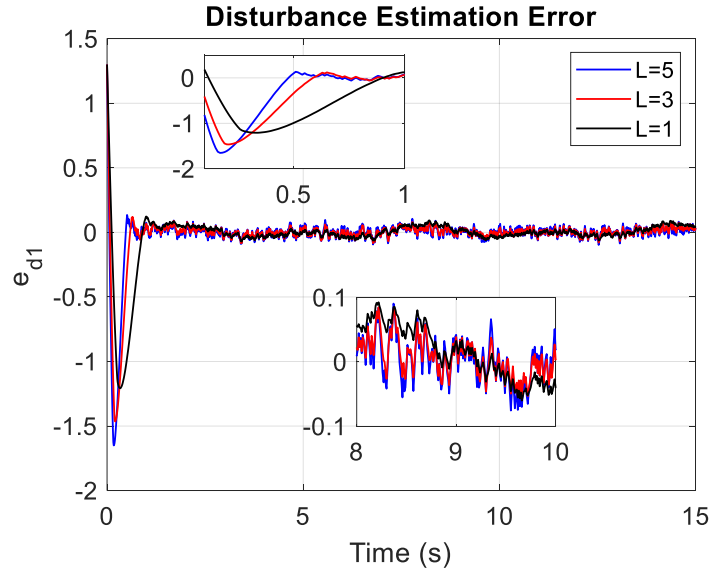


Figure 8. Influence of design parameters on observer performance.

To illustrate the influence of different design parameter values on the performance of the disturbance observer, three simulations are conducted with different values of the Lipschitz constant $L = 1, 3, 5$. The simulations are carried out in a measurement noise environment with a mean of 0 and a variance of $5e-3$, and the sampling time is set to be $t_s = 0.01[s]$ for practicality. Also, the initial value of the observer state and that of the system state are indicated to be different from each other, $\hat{d}_1(0) = z_{21}(0) = 0.5$, $x_1(0) = 1$. The result obtained is shown in Figure 8, which strongly agrees with the statement noted in **Remark 1**. Specifically, it is evident from Figure 8 that ($L = 1$) gives the longest convergence time, the smallest peaking phenomenon and is least susceptible to noise. Whereas ($L = 5$) takes the shortest amount of time for the estimation error to converge to zero but at the same time produces the largest peaking phenomenon and is most susceptible to noise. The most appropriate value is ($L = 3$), which represents a tradeoff between convergence time and sensitivity to noise and different initial values in tuning the observer parameters. Thus, it is concluded here that the greater Lipschitz constant L selection, the faster convergence of the disturbance observer yet more sensitive to noise and larger peaking phenomenon in the transition period as the initial value of the disturbance observer and that of the system are different.

Finally, to demonstrate the characteristic of nominal control performance preservation, a case study has been conducted with the conventional TSMC and the proposed DOBTSMC. In this study, almost all parameters are left to be the same as before except that the mismatched

disturbance disturbs the control system only after $t = 5[s]$. The simulation result is shown in Figure 9 below.

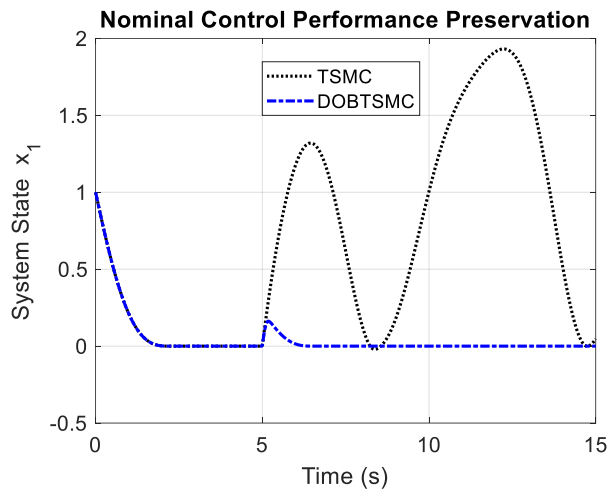


Figure 9. Nominal performance preservation capability of the proposed controller.

It is noticeable that the system state trajectory of the conventional TSMC and that of the proposed control algorithm are identical before $t = 5[s]$ and only start to diverge after that. This implies that the disturbance observer does not spoil the nominal control performance of the control system as the disturbance is absent, which is illustrative of **Remark 4**.

In summary, this section uses a numerical example to verify the effectiveness of the proposed control algorithm as it is compared with other controllers. The numerical study also helps investigate several characteristics of the proposed controller, namely the ability to estimate and suppress disturbances, chattering attenuation and nominal control performance. Also, this section illustrates the importance of control design parameter in the condition of measurement noise and large sampling time.

4.2 Case Study 2: Stabilizing an Electro Hydrostatic Actuator System in Simulation

The finite-time DOB-based chattering-free full-order TSMC developed previously is applied to stabilize an electro hydrostatic actuator (EHA) system in this section.

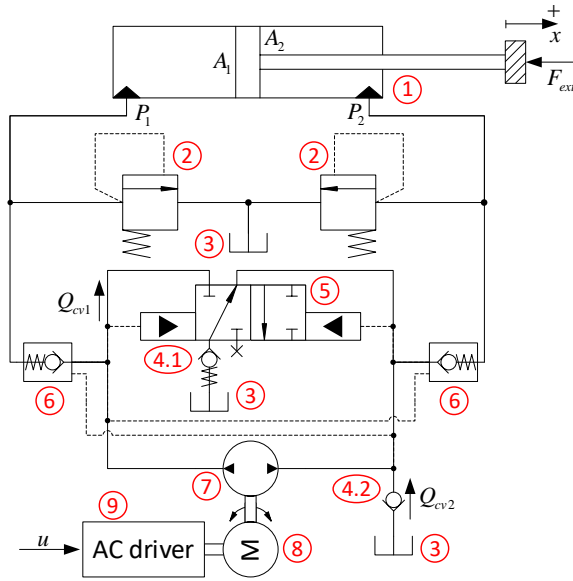


Figure 10. Schematic diagram of the EHA system.

Table 1. Major components in the considered EHA system

No.	Device	No.	Device
1	Hydraulic cylinder	5	Directional valve
2	Relief valves	6	Pilot check valve
3	Reservoir	7	Hydraulic pump
4.1	Check valves	8	AC motor
4.2		9	AC motor driver

The EHA studied in this section is illustrated in Figure 10 and its components are listed in Table 1. In the hydraulic circuit, cylinder (1) is driven by the valve system and the hydraulic pump (7), which is actuated by the AC motor (8). The flow discrepancy between the bore- and rod- chamber is automatically compensated by the check valve (4.1) and (4.2) with the support of the pilot-operated directional valve (5). In cooperation with two check valves (6), the hydraulic pump regulates the fluid flow inside the hydraulic circuit, thus controlling the movement of the cylinder.

Parameters of the EHA system to be used for mathematical modeling are defined as in Table 2 below.

Table 2. List of parameters used to model the EHA system.

Symbol	Quantity and Unit
x	Displacement of the cylinder. [m]
P_1, P_2	Pressures inside the cylinder chambers. [Pa]
A_1, A_2	Bore- and rod- side areas of the cylinder. [m ²]
m	Relative mass of the motion system. [kg]
V_{10}, V_{20}	Initial volumes of chamber 1 and 2. [m ³]
$V_{1r} = V_{10} + A_1 x$	Active volume of chamber 1. [m ³]
$V_{2r} = V_{20} - A_2 x$	Active volume of chamber 2. [m ³]
β_e	Effective bulk modulus of the fluid. [Pa]
C_{Li}	Internal leakage coefficient. [m ³ /(sPa)]
D	Displacement of the pump. [m ³ /rad]
K_{dr}	Control gain of the motor driver. [rad/(sV)]
η_V	Volumetric efficiency of the pump.
u	Driving voltage of the motor driver. [V]
$b_1, b_2, \gamma_2, \gamma_3$	Positive constants in the system model.
δ_2	Lumped disturbance in force dynamics. [N]
δ_{31}, δ_{32}	Lumped disturbances in pressure dynamics. [N/s]

Referred to [52], the dynamic model of the EHA system studied here consists of force dynamics and pressure dynamics as follows.

The force dynamics of the actuator is expressed as

$$m\ddot{x} = P_1 A_1 - P_2 A_2 + f_{Fr} + \delta_2 \quad (71)$$

where f_{Fr} denotes a lumped friction force [53, 54] and is approximated as a differential function of the form:

$$\begin{cases} f_{Fr} = -b_1 \dot{x} - b_2 \tanh(\dot{x}) \\ \tanh(\dot{x}) = \frac{1 - e^{-\gamma_2 \dot{x}}}{1 + e^{-\gamma_2 \dot{x}}} \end{cases} \quad (72)$$

and δ_2 represents a force disturbance that might include external forces and unmodeled force dynamics.

Governed by the continuity law [55], the pressure dynamics of the actuator are:

$$\begin{cases} V_{1t}\dot{P}_1 = \beta_e (\eta_V DK_{dr}u - A_1\dot{x} - C_{Li}(P_1 - P_2) - Q_{cv1}) + \delta_{31} \\ V_{2t}\dot{P}_2 = \beta_e (-\eta_V DK_{dr}u + A_2\dot{x} + C_{Li}(P_1 - P_2) + Q_{cv2}) + \delta_{32} \end{cases} \quad (73)$$

where Q_{cv1} and Q_{cv2} are respectively the flow in the check valve (4.1) and (4.2) and described as

$$\begin{cases} Q_{cv1} = -\dot{x}(A_1 - A_2)\text{sm}(-\dot{x}) \\ Q_{cv2} = \dot{x}(A_1 - A_2)\text{sm}(\dot{x}) \\ \text{sm}(\ast) = (1 + e^{-\gamma_3\ast})^{-1} \end{cases} \quad (74)$$

By defining the system state as $[x_1, x_2, x_3]^T = [x, \dot{x}, (P_1A_1 - P_2A_2)/m]^T$ and combining (71) to (74), the total dynamic system can be expressed in a state-space form as follows.

$$\begin{cases} \dot{x}_1 = x_2 \\ \dot{x}_2 = x_3 + d_1 \\ \dot{x}_3 = f + g u + d_2 \end{cases} \quad (75)$$

where the dynamic functions are specifically defined as

$$\begin{cases} f = \frac{\beta_e}{m} \left[\frac{A_1}{V_{1t}} (-A_1 + (A_1 - A_2)\text{sm}(-x_2)) - \frac{A_2}{V_{2t}} (A_2 + (A_1 - A_2)\text{sm}(x_2)) \right] x_2 \\ g = \frac{\beta_e \eta_V DK_{dr}}{m} \left(\frac{A_1}{V_{1t}} + \frac{A_2}{V_{2t}} \right) \\ d_1 = \frac{1}{m} (f_{Fr} + \delta_2) \\ d_2 = -\frac{\beta_e}{m} C_{Li} (P_1 - P_2) \left(\frac{A_1}{V_{1t}} + \frac{A_2}{V_{2t}} \right) + \frac{A_1 \delta_{31}}{m V_{1t}} - \frac{A_2 \delta_{32}}{m V_{2t}} \end{cases} \quad (76)$$

Information about disturbances existing in the system can be interpreted from the equation set (75) and (76) as follows. While d_1 represents a mismatched disturbance, d_2 is a matched one. The mismatched disturbance consists of the ratios of lumped friction f_{Fr} and δ_2 , the summation of external forces and unmodeled force dynamics, to the relative mass of the motion system m . Whereas the matched disturbance includes the ratios of internal leakages and pressure disturbances to m . It is assumed that these disturbances satisfy **Assumption 1** and **Assumption 2**.

Using (35), to estimate the mismatched disturbance d_1 , a finite-time disturbance observer can be designed as follows.

$$\begin{cases} \dot{z}_{12} = v_{12} + x_3 \\ v_{12} = -\lambda_{12} L_2^{1/4} |z_{12} - x_2|^{3/4} \text{sign}(z_{12} - x_2) - \mu_{12} (z_{12} - x_2) + z_{22} \\ \dot{z}_{22} = v_{22} \\ v_{22} = -\lambda_{22} L_2^{1/3} |z_{22} - v_{12}|^{2/3} \text{sign}(z_{22} - v_{12}) - \mu_{22} (z_{22} - v_{12}) + z_{32} \\ \dot{z}_{32} = v_{32} \\ v_{32} = -\lambda_{32} L_2^{1/2} |z_{32} - v_{22}|^{1/2} \text{sign}(z_{32} - v_{22}) - \mu_{32} (z_{32} - v_{22}) + z_{42} \\ \dot{z}_{42} = -\lambda_{42} L_2 \text{sign}(z_{42} - v_{32}) - \mu_{42} (z_{42} - v_{32}) \end{cases} \quad (77)$$

where $z_{12} = \hat{x}_2$, $z_{22} = \hat{d}_1$, $z_{32} = \hat{d}_1$, $z_{42} = \hat{d}_1$, and $L_2 > 0$, $\lambda_{j2}, \mu_{j2} > 0$ ($j=1, \dots, 4$).

A chattering-free full-order TSMC for the EHA system can be then designed based on (37) as:

$$\sigma = \dot{x}_3 + c_3 |x_3 + z_{22}|^{\alpha_3} \text{sign}(x_3 + z_{22}) + c_2 |x_2|^{\alpha_2} \text{sign}(x_2) + c_1 |x_1|^{\alpha_1} \text{sign}(x_1) + z_{32} \quad (78)$$

where c_i ($i=1, 2, 3$) are positive constants satisfying the polynomial $p^3 + c_3 p^2 + c_2 p + c_1$ is Hurwitz, and α_i ($i=1, 2, 3$) are chosen as (38). Accordingly, the control law is developed with the form:

$$u = g^{-1}(u_{eq} + u_n) \quad (79)$$

where the equivalent control u_{eq} is designed as

$$u_{eq} = -f - c_3 |x_3 + z_{22}|^{\alpha_3} \text{sign}(x_3 + z_{22}) - c_2 |x_2|^{\alpha_2} \text{sign}(x_2) - c_1 |x_1|^{\alpha_1} \text{sign}(x_1) - z_{32} \quad (80)$$

and the switching term u_n is defined as the same as in (22) and (23).

The nominal values of the system parameters were determined as in Table 3 [56].

Table 3. Nominal Value of the EHA System Parameters.

Parameter	Unit	Nominal (+ variance) Value
m	[kg]	9.32(+0.46)
A_1	[m ²]	$1.9635 \times 10^{-3} (+0.0982 \times 10^{-3})$
A_2	[m ²]	$1.2566 \times 10^{-3} (+0.0628 \times 10^{-3})$
V_{10}	[m ³]	$4.375 \times 10^{-4} (+0.219 \times 10^{-4})$
V_{20}	[m ³]	$2.88 \times 10^{-4} (+0.144 \times 10^{-4})$
β_e	[Pa]	5.34×10^8
K_{dr}	[rad/(sV)]	10π
$D_1 \triangleq \eta_V D$	[m ³ /rad]	$5.83 \times 10^{-7} (+0.29 \times 10^{-7})$
C_{Li}	[m ³ /(sPa)]	1.51×10^{-15}
b_1	[Ns/m]	258
b_2	[N]	532
γ_2		10
γ_3		15(+0.75)

The cylinder stroke length is 0.3[m], thus the working range of the actuator is set to be $x_1 \in [-0.15, 0.15][m]$. The pressure threshold of the relief valve is set to be 150[bar], meaning that $P_1, P_2 \in [0, 150 \times 10^5][Pa]$. To make the control task challenging and to examine the effectiveness of control algorithms, both matched and mismatched disturbances are deliberately assumed to be time-varying throughout the simulation period. Specifically, the force disturbance δ_2 and the pressure disturbances δ_{31}, δ_{32} are selected to be dependent on both time and system state as follows. $\delta_2 = -1000(0.2 + 0.5x_1 + x_2 + \sin(t))$, $\delta_{31} = -1000(0.1 + 3x_2 + \sin(t))$, and $\delta_{32} = 500(0.2 + x_2 + 2\sin(t))$. Also, for practicality, measurement noise and parameter uncertainty are added into the simulation. Specifically, the position and pressure measurements are subject to noises with a mean of 0 and a covariance of $\{0.0005[m], 3500[Pa], 3500[Pa]\}$ ($\sim 0.5\%$ of nominal values). Parameters used to design the controller are of nominal value. Whereas those parameters used to model the EHA system include variance ($\sim 5\%$ of nominal values), which are indicated in Table 3. The sampling time is set to be 1[ms].

In this section, TSMC and the proposed DOBTSMC are compared to verify the effectiveness of the proposed controller. Some control parameters are chosen to be the same

for both control algorithms, namely $c_1 = 318$, $c_2 = 500$, $c_3 = 270$, $T = 0.1$, and $\beta = (\rho_2 + k_T + \eta) = 3000$, $\alpha_i (i = 1, 2, 3)$ are designed as $\alpha_1 = 1/7$, $\alpha_2 = 1/5$, $\alpha_3 = 1/3$, following (38). For mismatched disturbance observation, the proposed DOB parameters are chosen as $L_2 = 500$, $\lambda_{12} = 30$, $\lambda_{22} = 55$, $\lambda_{32} = 30$, $\lambda_{42} = 5$, $\mu_{12} = 36$, $\mu_{22} = 18$, $\mu_{32} = 6$, $\mu_{42} = 1$.

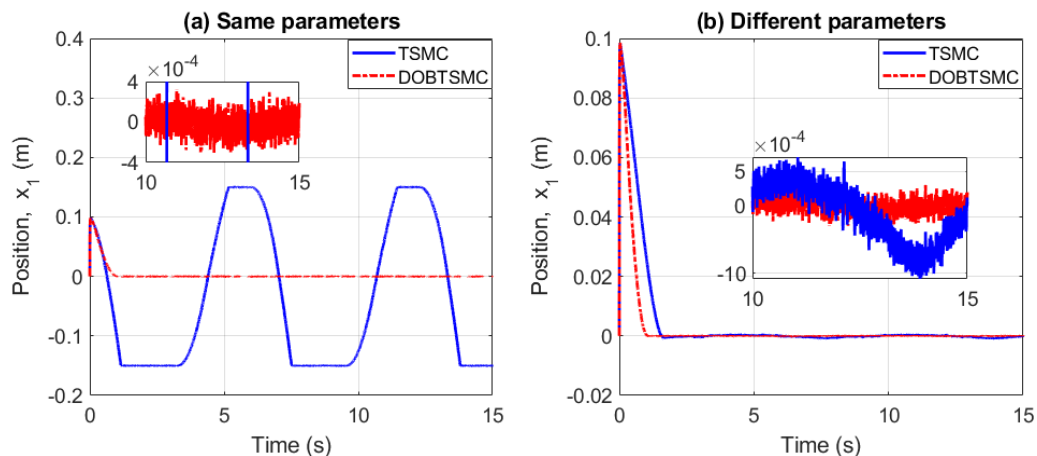


Figure 11. Response position trajectories in case of same (a) and different (b) control parameters.

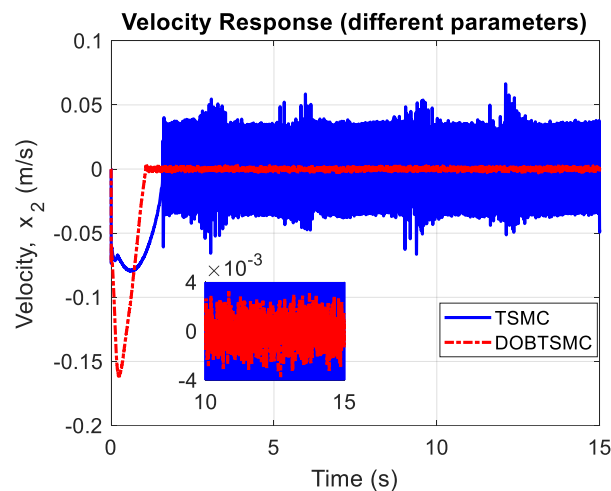


Figure 12. Response velocity trajectories of EHA system.

The position and velocity responses of the EHA system are shown in Figure 11 and Figure 12. While Figure 11 presents the position trajectory of all control algorithms, Figure 12 depicts the velocity trajectory of the ESOSMC and the DOBTSMC. Clearly seen in Figure 11a, under the same-control-parameter design condition, the TSMC is unable to stabilize the EHA system, which is subject to both mismatched and matched disturbances. Whereas the proposed control algorithm can achieve a high accuracy of ± 0.4 [mm]. Hence, the TSMC control parameters

need to be reselected for better comparison. The design parameters of DOBTSMC are kept to be the same, while those parameters of the TSMC are altered as: $c_1 = 3816$, $c_2 = 6000$, and $c_3 = 270$. The result is then shown in Figure 11b. Clearly, even though the performance of TSMC has been significantly improved after increasing control parameters, the closed-loop dynamics is still affected by the mismatched disturbance. In other words, TSMC cannot suppress the influence of mismatched disturbances. This demonstrates the superiority of the proposed controller over the conventional one. Figure 12 shows that while the DOBTSMC can drive the system velocity to a bounded region of ± 4 [mm/s] around the equilibrium point, a serious chattering phenomenon is seen for the TSMC. This can be explained as large control design parameters amplify the measurement noise and degrade the control performance. Besides, no overshoot and relatively fast response are seen for the proposed control algorithm.

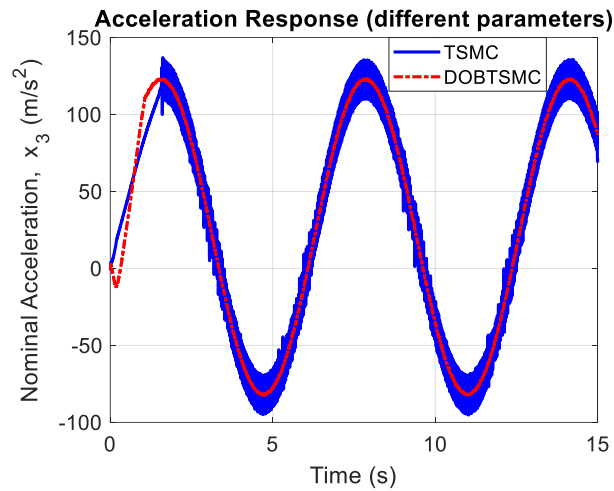


Figure 13. Response nominal acceleration trajectories of the EHA system.

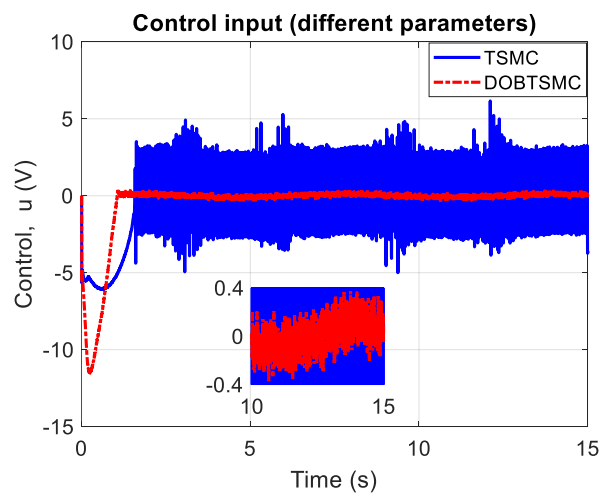


Figure 14. Response control signals of the EHA system.

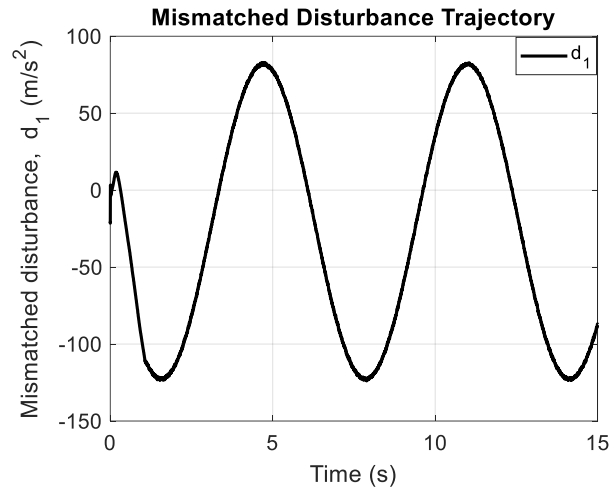


Figure 15. Mismatched disturbance existing in the EHA system.

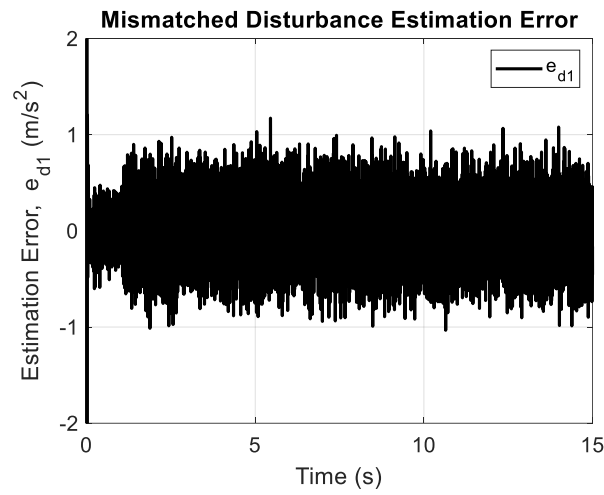


Figure 16. Mismatched disturbance estimation errors of the proposed controller.

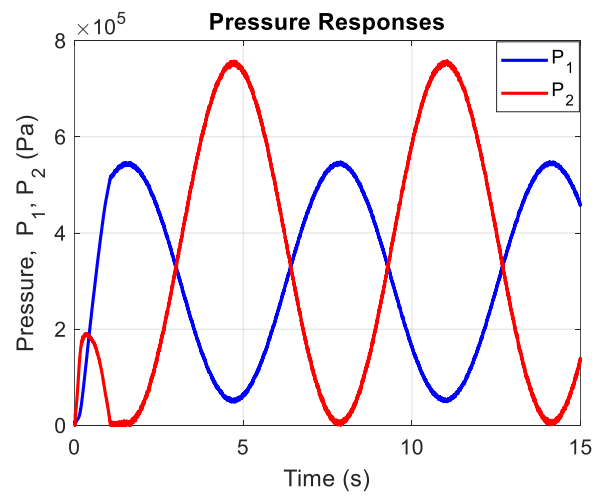


Figure 17. Response chamber pressures for the DOBTSMC case.

One can observe that the response nominal acceleration signal x_3 seen in Figure 13 is opposite in patterns with the mismatched disturbance d_1 in Figure 15 to stabilize the system states $x_{1,2}$, which agrees with the previous numerical study. However, severe chattering effects exist in the TSMC case for the same large-control-design-parameter reason discussed above. Under the condition of measurement noise and parameter uncertainty, the control effort generated by the proposed controller suffers a chattering phenomenon with a magnitude of $0.4[V]$, which is shown in Figure 14.

Figure 16 illustrates the performance of the proposed control algorithm in estimating mismatched disturbances. The accuracy it delivers is around $\pm 1[m/s^2](\sim 1\%)$, thus contributing to the higher performance in system stabilization. That said, there is a chattering phenomenon existing in the disturbance estimation due to measurement noise. This downgrades the disturbance estimation performance and consequently the performance of the control system as a whole. Finally, Figure 17 records the response pressures in the EHA system for the DOBTSMC case.

In summary, this section partly reflects the effectiveness of the proposed control algorithm in practice as it is employed to stabilize an EHA system, which is subject to both time-varying mismatched and matched disturbances. This simulation study also takes into account the negative impact of measurement noise and parameter uncertainty to verify the robustness of the proposed control algorithm. Overall, the mismatched disturbance is accurately estimated, and the estimation result is used to suppress the undesired influence on the control system. The proposed controller delivers a satisfactory control performance.

4.3 Case Study 3: Voltage Control for Bidirectional DC-DC Converter

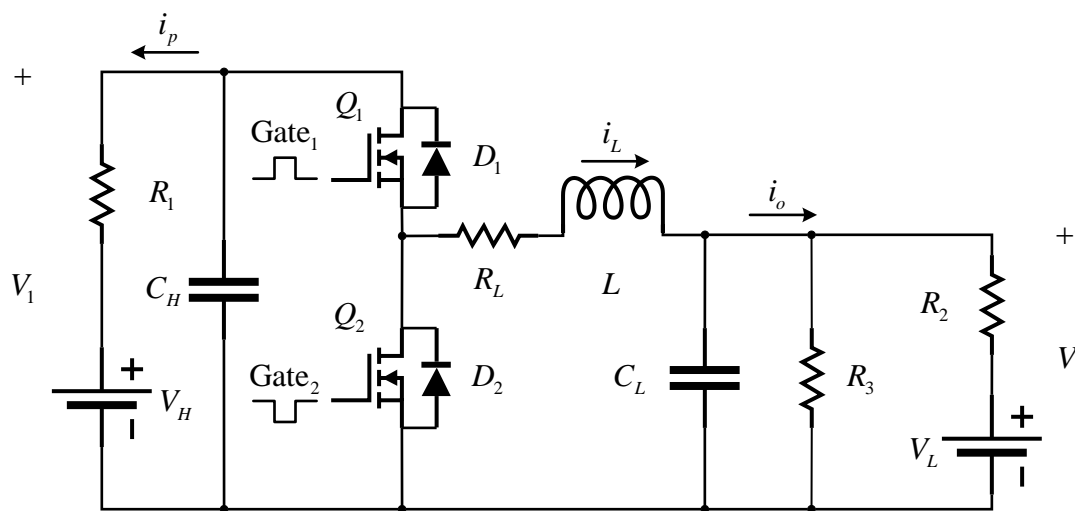


Figure 18. Circuit diagram of a bidirectional DC-DC converter.

Based on [57], the circuit description and modeling of a typical PWM-based bidirectional DC-DC converter are presented as follows. The bidirectional DC-DC converter structure is shown in Figure 18, where V_H and V_L represent the high-side and low-side dc voltage source, respectively. The inductor current i_L , input current i_p , and output current i_o can flow in both directions. Resistor R_1 represents either high-side source internal resistance in charging and discharging modes or load in boost resistive load application. Similarly, resistor R_2 represents either low-side source internal resistance for both charging and discharging modes or load in buck resistive load application. Resistor R_3 represents the resistive load that can vary during operation. Capacitor C_H and C_L indicate the high-side and low-side capacitor, respectively. Two active switches, Q_1 and Q_2 , are controlled by a complementary gating control signal Gate_1 and Gate_2 separately. R_L and R_{dson} represents the inductor parasitic resistance and the MOSFET turn-on resistance, respectively. Thus, there are three energy storage components including input capacitor C_H , output capacitor C_L , and inductor L .

With this configuration, the derived power plant can be utilized for battery charging and discharging modes or buck/ boost resistive load applications, since all these cases can employ the same equivalent circuit.

Control-Oriented Modeling the Bidirectional DC-DC Converter

Since the two active switches, Q_1 and Q_2 are controlled complementarily, no matter which operating modes, either battery charging or discharging, there are always two states, state 1: Q_1 ON - Q_2 OFF or state 2: Q_1 OFF - Q_2 ON.

The first state 1, Q_1 ON - Q_2 OFF, is shown in Figure 19 below.

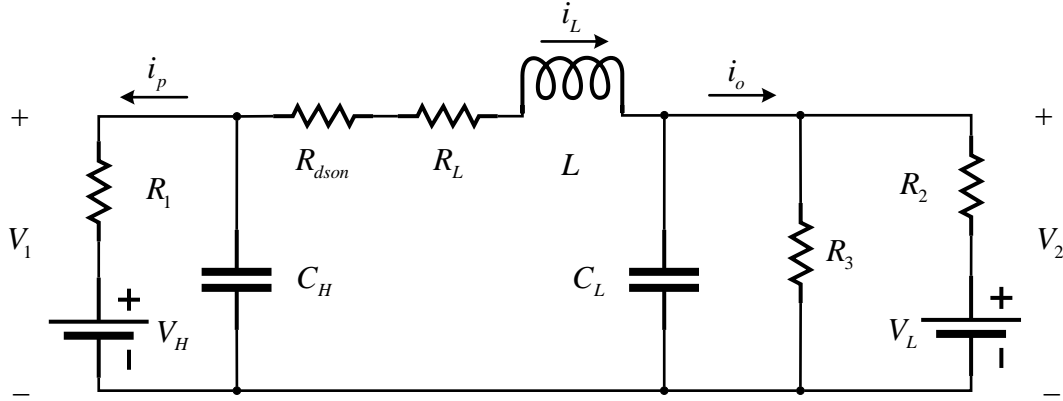


Figure 19. Equivalent circuit diagram of the state 1: Q_1 ON - Q_2 OFF

There are three energy storage components including inductor current i_L , high-side capacitor voltage V_1 , and low-side capacitor voltage V_2 . The governing equation for inductor voltage across the inductor L and the capacitor currents through the two capacitors are given as follows.

$$\begin{cases} L\dot{i}_L = -i_L R_{eq} + V_1 - V_2 \\ C_H \dot{V}_1 = -i_L - \frac{V_1 - V_H}{R_1} \\ C_L \dot{V}_2 = i_L - \frac{V_2 - V_L}{R_2} - \frac{V_2}{R_3} \end{cases} \quad (81)$$

where $R_{eq} = R_{dson} + R_L$ represents the equivalent resistance of R_{dson} and R_L since they are placed in series.

At the second state, Q_1 OFF - Q_2 ON, the converter equivalent circuit can be illustrated in Figure 20 below.

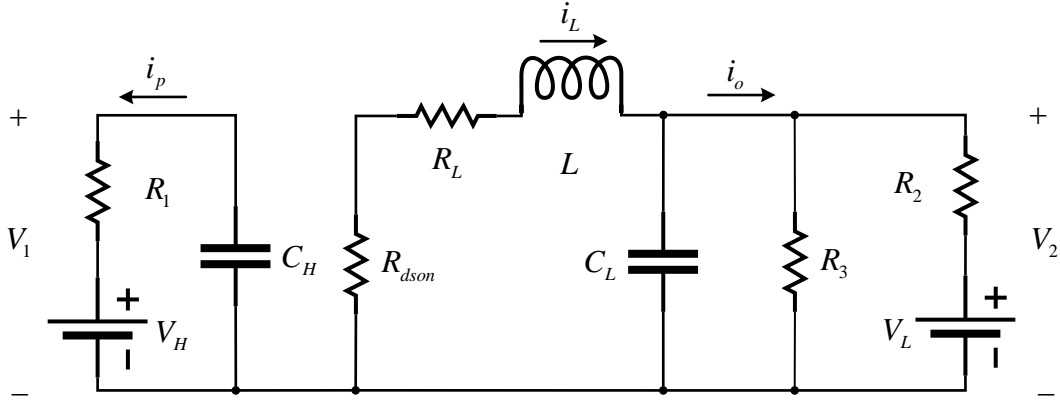


Figure 20. Equivalent circuit diagram of state 2: Q_1 OFF - Q_2 ON.

The governing equation set for this state is given by:

$$\begin{cases} L\dot{i}_L = -i_L R_{eq} - V_2 \\ C_H \dot{V}_1 = -\frac{V_1 - V_H}{R_1} \\ C_L \dot{V}_2 = i_L - \frac{V_2 - V_L}{R_2} - \frac{V_2}{R_3} \end{cases} \quad (82)$$

where, again, $R_{eq} = R_{dson} + R_L$ represents the equivalent resistance of R_{dson} and R_L .

Based on the equation set (81) and (82), an average system model is derived as below.

$$\begin{cases} L\dot{i}_L = -i_L R_{eq} + \mu V_1 - V_2 \\ C_H \dot{V}_1 = -\mu i_L - \frac{V_1 - V_H}{R_1} \\ C_L \dot{V}_2 = i_L - \frac{V_2 - V_L}{R_2} - \frac{V_2}{R_3} \end{cases} \quad (83)$$

where $\mu \in [0,1]$ denotes the input duty cycle taken as the control signal of PWM.

Although this circuit configuration offers different operating modes such as battery charging and discharging or resistive load applications, this section will only present the case of voltage control at the low side. Its objective is to demonstrate the effectiveness of the proposed control algorithm developed in the previous section. Other cases, which are important for applications such as in an electric vehicle, are left for future work.

In this scenario, let V_2 be the controlled output. Three disturbances that exist in the system from the controlling point of view are presented as follows.

- 1) Perturbation in duty cycle: $\mu = \bar{\mu} + \Delta\mu$
- 2) Load resistance variation: $R_3 = \bar{R}_3 + (R_3 - \bar{R}_3)$

3) Low-side voltage uncertainty: $V_L = \bar{V}_L + \Delta V_L$

Here, $\bar{\mu}$ denotes the nominal input duty cycle, $\Delta\mu$ denotes the perturbation in the duty cycle, \bar{R}_3 represents the nominal load resistance, \bar{V}_L denotes the nominal low-side voltage, and ΔV_L represents the uncertainty in the low-side voltage.

Let $x_1 = e = V_2 - V_r$, where V_r denotes the desired output voltage. The system model can be rewritten as follows.

$$\begin{aligned}\dot{x}_1 &= \dot{e} = \dot{V}_2 = \frac{1}{C_L} i_L - \frac{1}{R_2 C_L} (V_2 - V_L) \\ &= \frac{1}{C_L} i_L - \frac{1}{C_L} \left(\frac{1}{R_2} + \frac{1}{\bar{R}_3} \right) V_2 + \frac{1}{R_2 C_L} \bar{V}_L - \frac{1}{C_L} \left(\frac{1}{R_3} - \frac{1}{\bar{R}_3} \right) V_2 + \frac{1}{R_2 C_L} \Delta V_2 \\ &= x_2 + d_1\end{aligned}\quad (84)$$

where $x_2 = i_L/C_L - (V_2/C_L)(1/R_2 + 1/\bar{R}_3) + \bar{V}_L/(R_2 C_L)$ represents the second system state, and $d_1 = -(V_2/C_L)(1/R_3 - 1/\bar{R}_3) + \Delta V_L/(R_2 C_L)$ denotes the first disturbance of the system.

Differentiating x_2 yields:

$$\begin{aligned}\dot{x}_2 &= \frac{1}{C_L} \dot{i}_L - \frac{1}{C_L} \left(\frac{1}{R_2} + \frac{1}{\bar{R}_3} \right) \dot{V}_2 \\ &= \frac{1}{LC_L} (-i_L R_{eq} + \bar{\mu} V_1 + \Delta\mu V_1 - V_2) - \frac{1}{C_L} \left(\frac{1}{R_2} + \frac{1}{\bar{R}_3} \right) (x_2 + d_1) \\ &= -\frac{R_{eq}}{L} \left(\frac{1}{C_L} i_L - \frac{1}{C_L} \left(\frac{1}{R_2} + \frac{1}{\bar{R}_3} \right) V_2 + \frac{1}{R_2 C_L} V_L \right) - \frac{R_{eq}}{LC_L} \left(\frac{1}{R_2} + \frac{1}{\bar{R}_3} \right) V_2 \\ &\quad + \frac{R_{eq}}{R_2 LC_L} V_L + \frac{1}{LC_L} \bar{\mu} V_1 + \frac{1}{LC_L} \Delta\mu V_1 - \frac{1}{LC_L} V_2 - \frac{1}{C_L} \left(\frac{1}{R_2} + \frac{1}{\bar{R}_3} \right) (x_2 + d_1) \\ &= -\left(\frac{R_{eq}}{L} + \frac{1}{C_L} \left(\frac{1}{R_2} + \frac{1}{\bar{R}_3} \right) \right) x_2 - \frac{1}{LC_L} \left(R_{eq} \left(\frac{1}{R_2} + \frac{1}{\bar{R}_3} \right) + 1 \right) x_1 + \frac{R_{eq}}{R_2 LC_L} V_L \\ &\quad + \frac{1}{LC_L} \left(\bar{\mu} V_1 - \left(R_{eq} \left(\frac{1}{R_2} + \frac{1}{\bar{R}_3} \right) + 1 \right) V_r \right) \\ &\quad - \frac{1}{C_L} \left(\frac{1}{R_2} + \frac{1}{\bar{R}_3} \right) d_1 + \frac{1}{LC_L} \Delta\mu V_1\end{aligned}\quad (85)$$

This expression can be further reduced to:

$$\dot{x}_2 = f + u + d_2 \quad (86)$$

where:

$$\begin{cases} f = -\left(\frac{R_{eq}}{L} + \frac{1}{C_L}\left(\frac{1}{R_2} + \frac{1}{R_3}\right)\right)x_2 - \frac{1}{LC_L}\left(R_{eq}\left(\frac{1}{R_2} + \frac{1}{R_3}\right) + 1\right)x_1 + \frac{R_{eq}}{R_2 LC_L}V_L \\ u = \frac{1}{LC_L}\left(\bar{\mu}V_1 - \left(R_{eq}\left(\frac{1}{R_2} + \frac{1}{R_3}\right) + 1\right)V_r\right) \\ d_2 = -\frac{1}{C_L}\left(\frac{1}{R_2} + \frac{1}{R_3}\right)d_1 + \frac{1}{LC_L}\Delta\mu V_1 \end{cases} \quad (87)$$

In the above equation set, f is interpreted as the system dynamics, d_2 represents the second disturbance of the system, and u represents the virtual control input, from which the actual command duty cycle can be calculated as:

$$\bar{\mu} = \frac{1}{V_1}\left(LC_L u + \left(R_{eq}\left(\frac{1}{R_2} + \frac{1}{R_3}\right) + 1\right)V_r\right) \quad (88)$$

By combining (84) and (86), one can obtain the following canonical form:

$$\begin{cases} \dot{x}_1 = x_2 + d_1 \\ \dot{x}_2 = f + u + d_2 \end{cases} \quad (89)$$

Thus, the problem of voltage tracking control for a bidirectional DC-DC converter now is transformed into the problem of stabilizing a second-order nonlinear system. The canonical format is more convenient for nonlinear control algorithm applications than the original governing equations. In this system, d_1 enters the system in a different channel from the control input u . Thus, d_1 can be interpreted as a mismatched disturbance. Whereas, d_2 represents a matched one.

The primary objective here is to force the system state x_1 to converge to the equilibrium quickly and accurately. To achieve this objective, the disturbance observer-based TSMC developed in the previous section is applied as follows. First, the finite-time disturbance observer is designed as:

$$\begin{cases} \dot{z}_{11} = v_{11} + x_2 = \varphi_{11}(z_{11} - x_1) + z_{21} + x_2 \\ \dot{z}_{21} = v_{21} = \varphi_{21}(z_{21} - v_{11}) + z_{31} \\ \dot{z}_{31} = \varphi_{31}(z_{31} - v_{21}) \end{cases} \quad (90)$$

where φ_{j1} are the functions:

$$\varphi_{j1}(s) = -\lambda_{j1} L_1^{1/(4-j)} |s|^{(3-j)/(4-j)} \text{sign}(s) - \mu_{j1}(s) \quad (91)$$

and $z_{11} = \hat{x}_1$, $z_{21} = \hat{d}_1$, $z_{31} = \hat{d}_1$, $L_1 > 0$, $\lambda_{j1}, \mu_{j1} > 0$, $j=1,2,3$. Next, a chattering-free full-order TSMC can be employed as:

$$\sigma = \dot{x}_2 + c_2 |x_2 + z_{21}|^{\alpha_2} \text{sign}(x_2 + z_{21}) + c_1 |x_1|^{\alpha_1} \text{sign}(x_1) + z_{31} \quad (92)$$

where c_1, c_2 are selected positive constants such that the polynomial $p^2 + c_2 p + c_1$ is Hurwitz. α_1 and α_2 are chosen according to the following manner:

$$\begin{cases} \alpha_2 = \alpha, \alpha \in (1-\varepsilon, 1), \varepsilon \in (0, 1) \\ \alpha_1 = \frac{\alpha_2}{2-\alpha_2} \end{cases}$$

The virtual control input u is then designed based on the sliding surface as:

$$u = u_{eq} + u_n \quad (93)$$

where u_{eq} denotes the equivalent control signal with the form of:

$$u_{eq} = -f - c_2 |x_2 + z_{21}|^{\alpha_2} \text{sign}(x_2 + z_{21}) - c_1 |x_1|^{\alpha_1} \text{sign}(x_1) - z_{31} \quad (94)$$

and u_n represents the switching term being defined and filtered as:

$$\begin{cases} \dot{u}_n + T u_n = v \\ v = -(\rho_2 + k_T + \eta) \text{sign}(\sigma) \end{cases} \quad (95)$$

where the design parameters T, k_T, η are defined as the same as below (7). The actual command duty cycle fed into the system is then calculated using (88).

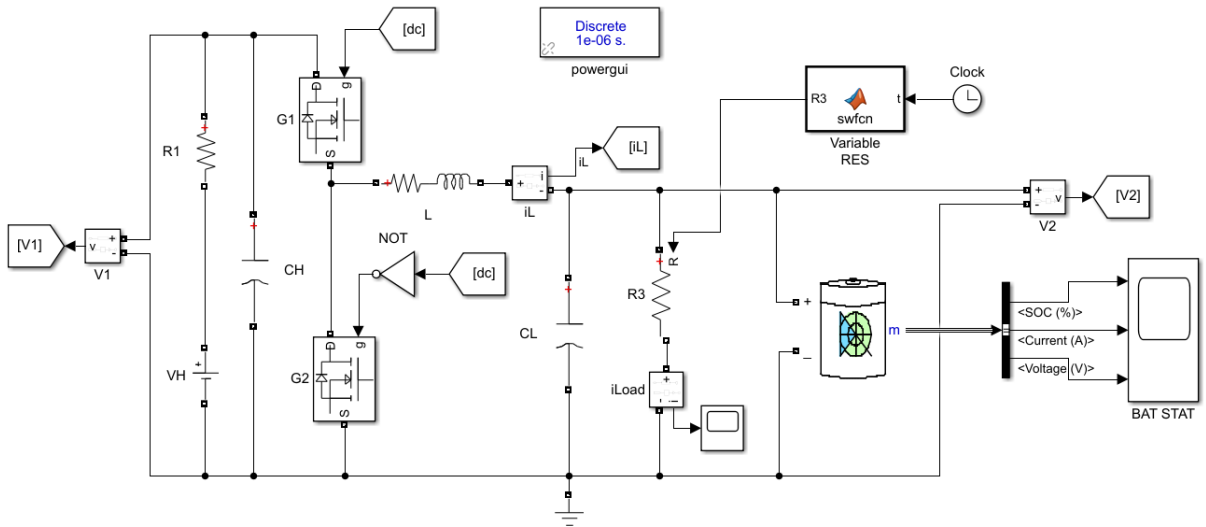


Figure 21. MATLAB-Simscape modeling of the system.

The simulation is conducted in the MATLAB-Simscape environment. The system is modeled as in Figure 21, wherein the simulation sampling time is set to be $1e-6[s]$, and the solver is selected to be the fixed-step ODE4 (Runge-Kutta). The battery is selected with the nominal voltage of $12[V]$, a capacity of $5.4[Ah]$, 50% State-Of-Charge (SOC), which gives around $12.8[V]$ of initial voltage, and an internal resistance of $0.022222[\Omega]$. Other settings are left as default. The system parameters are selected based on [31] and shown in Table 4 below.

Table 4. Nominal Values of the Bidirectional Converter Parameters

Parameter	Unit	Value
V_H	[V]	24
\bar{V}_L	[V]	12
C_H	[F]	$1000e-6$
C_L	[F]	$1000e-6$
L	[H]	$4.7e-3$
$R_{eq} = R_L + R_{dson}$	$[\Omega]$	$0.03 + 8.7e-3$
R_1	$[\Omega]$	0.03
R_2	$[\Omega]$	0.022222
\bar{R}_3	$[\Omega]$	3
$\Delta\mu$		$0.01\sin(200\pi t)$

In this simulation study, to make the controlling task challenging, the resistance disturbance in the resistor R_3 is set to be load-step resistance that changes from $3[\Omega]$ to $6[\Omega]$ after $t = 0.5[s]$. The perturbation in the duty cycle is set to be an ac signal of 100Hz with a magnitude of 0.01. The desired output voltage is set to be $V_r = 14[V]$.

The design parameters of the disturbance observer are selected as: $L_1 = 1e5$, $\lambda_{11} = 120$, $\lambda_{21} = 640$, $\lambda_{31} = 20$, $\mu_{11} = 6$, $\mu_{21} = 32$, $\mu_{31} = 1$. For the TSMC, the control parameters are chosen as: $c_1 = 1.5e5$, $c_2 = 0.5e5$, $\alpha_2 = 1/3$, $\alpha_1 = \alpha_2 / (2 - \alpha_2) = 1/5$. To verify the effectiveness of the chattering alleviation method, the simulation study is first conducted using the unfiltered term $u_n = -\beta \text{sign}(\sigma)$ and later compared with the results obtained by using the low-pass filter like method as in (95), where $T = 50$, and $\beta = (\rho_2 + k_T + \eta) = 5e7$.

Simulation Results

The simulation results are shown in Figure 22 to Figure 26.

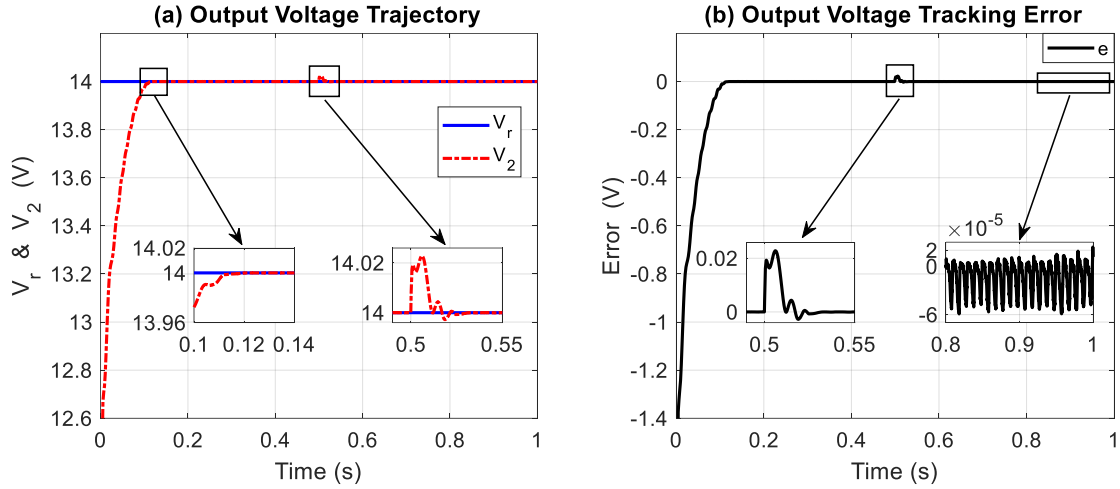


Figure 22. Output voltage response (a) and voltage tracking error (b) of the converter.

Figure 22 presents the output voltage response of the converter using the proposed controller. On the one hand, Figure 22a shows that the time of convergence is about $0.12[s]$ as the resistive load is $3[\Omega]$. At $t = 0.5[s]$, this resistive load increases to $6[\Omega]$, and it takes approximately $0.03[s]$ for the system to reach the state of stabilization. This indicates that the proposed control algorithm possesses a fast response characteristic. On the other hand, Figure 22b demonstrates that the steady-state tracking error is about $6e-5[V]$, which is around 0.00043% the desired value. This indicates that the proposed controller achieves high accuracy tracking performance. Also, no overshoot is seen in the voltage response.

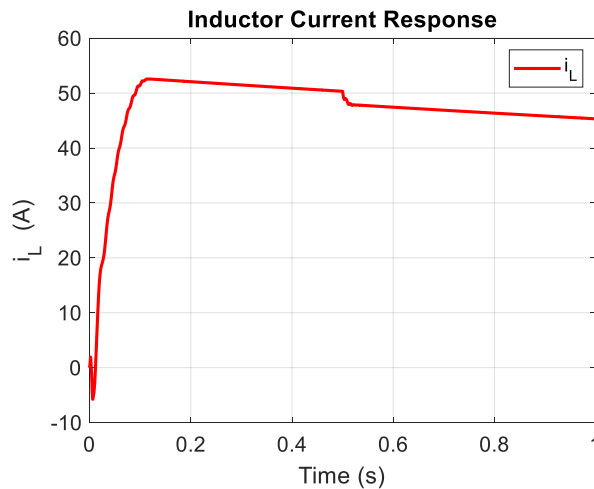


Figure 23. Inductor current response of the converter.

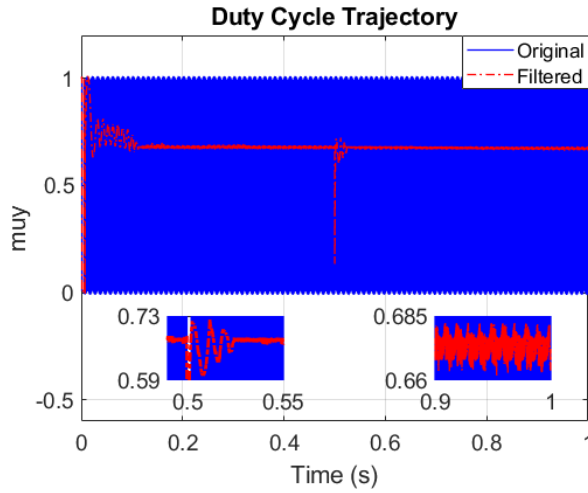


Figure 24. Duty cycle response of the converter: Original and Filtered.

Inductor current response is illustrated in Figure 23, in which the current value appears to decrease over time. This happens because the internal resistance of the battery gradually increases during charging. The branch voltage difference, $\Delta V = V_r - V_{\text{BAT}} = 14 - 12.8 = 1.2[\text{V}]$ will be divided by the small battery internal resistance, $R_{\text{BAT}} = R_2 = 0.022222[\Omega]$, to create such a high branch current value and consequently contribute to the high inductor current seen in Figure 23. The duty cycle trajectories before and after filtering are shown in Figure 24, which illustrates the severe chattering phenomenon of the signum function. To alleviate this chattering effect, the lowpass-filter like method (95) is applied. However, the chattering effect still exists in the duty cycle trajectory with a magnitude of around 0.025, indicating that the control system has not reached the level of chattering-free. This problem can be explained as follows. The small-value of components (L and C_L) that appear in the denominator of a fraction in system modeling and large-value control parameters used in controller design lead to the amplification of the chattering effect that exists in any part of the control system. This means unless the control system is chattering-free in every part, the control signal can never be free from chattering even though the switching control term has been filtered.

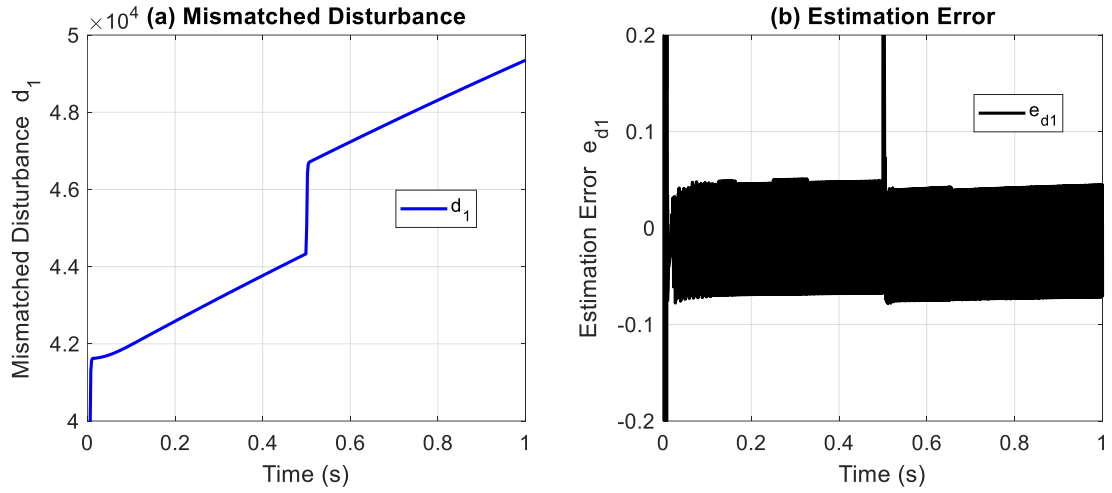


Figure 25. Mismatched disturbance (a) and its estimation error (b).

Figure 25 shows the mismatched disturbance existing in the system and the estimation error delivered by the disturbance observer. Clearly from Figure 25a, the mismatched disturbance is time-varying, not constant, meaning that its derivative will not diminish even when the system reaches the steady-state condition. The mismatched disturbance is of large value, $[4.1e4 \sim 4.9e4]$, which implies a large observer design parameter requirement. Whereas, Figure 25b demonstrates the effectiveness of the proposed disturbance observer with an estimation error of $[\pm 0.08 \sim 0.000178\%]$. Although high accuracy is seen in the performance of the observer, it still exhibits a chattering phenomenon. This subsequently contributes to the chattering effect seen in the control signal.

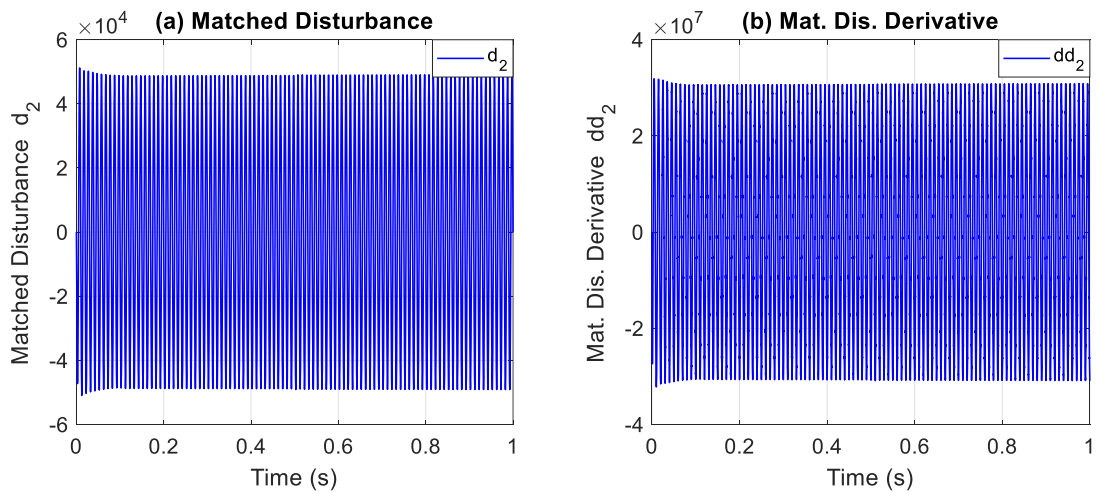


Figure 26. Matched disturbance (a) and its derivative (b) existing in the system.

Figure 26 presents the matched disturbance and its derivative existing in the system. Restate the formula of the switching parameter as follows. $\beta = (\rho_2 + k_T + \eta)$, where $\eta > 0$, $|\dot{d}_2| \leq \rho_2$, and $k_T \geq T\phi_2$, $|d_2| \leq \phi_2$, $T = 50$. The signals illustrated in Figure 26 and these above expressions explain why the magnitude of the control parameter, $\beta = (\rho_2 + k_T + \eta) = 5e7$ was set to be large to overcome the influence of matched disturbances. This figure could have been larger if the equivalent control law u_{eq} were not modified as follows. As the matched disturbance d_2 relates to the mismatched disturbance d_1 by the following relationship (87):

$$d_2 = -\frac{1}{C_L} \left(\frac{1}{R_2} + \frac{1}{R_3} \right) d_1 + \frac{1}{LC_L} \Delta \mu V_1 \quad (96)$$

the equivalent control u_{eq} (94) can be modified to lift the burden on the switching control term u_n as:

$$u_{eq} = -f - c_2 |x_2 + z_{21}|^{\alpha_2} \text{sign}(x_2 + z_{21}) - c_1 |x_1|^{\alpha_1} \text{sign}(x_1) - z_{31} - z_{22} \quad (97)$$

where:

$$z_{22} = \hat{d}_2 = -\frac{1}{C_L} \left(\frac{1}{R_2} + \frac{1}{R_3} \right) \hat{d}_1 = -\frac{1}{C_L} \left(\frac{1}{R_2} + \frac{1}{R_3} \right) z_{21} \quad (98).$$

In summary, this section introduces a new method of control-oriented modeling a bidirectional DC-DC converter to the canonical form so that it is more convenient for applying model-based nonlinear control algorithms. This method also considers and isolates three types of different disturbances and then organizes them into two more general types, namely matched and mismatched disturbances. However, the existence of the multiplication, LC , in the denominator of the virtual control input u (87) forces the virtual control magnitude u to be large. Consequently, the control parameters must be also high to produce such a large virtual control signal. Thus, it is more difficult to tune the control parameters properly. Large control parameters also amplify the undesired chattering phenomenon in the control system and makes it seem impossible to reach the state of chattering-free. On the bright side, this section demonstrates that the proposed control algorithm can deliver fast and accurate tracking performance to the bidirectional DC-DC converter, which is subject to both matched and mismatched disturbances. Nonetheless, the practicality of the proposed controller must be evaluated via rigorous experiments. Also, different working modes such as buck/boost

switching should be considered to fully assess the performance and robustness of the proposed controller.

4.4 Case study 4: Experimental Validation on an Electro Hydrostatic Actuator (EHA) System

This section aims to evaluate the effectiveness of the proposed control algorithm in controlling the displacement of an EHA system via an experimental setup. The information of the system including system description, basic working principle, mathematical modeling and system parameters can be found in Section 4.2. The total dynamic system is restated here for later use. The system states are defined as:

$$[x_1, x_2, x_3]^T = \left[x, \dot{x}, \frac{P_1 A_1 - P_2 A_2}{m} \right]^T \quad (99)$$

where x and \dot{x} represent the displacement and velocity of the system. P_1 and P_2 are pressures inside the cylinder chambers. A_1 and A_2 are the bore-side and rod-side areas of the cylinder. m is the relative mass of the motion system. Differentiating the system states yields the total dynamic system as follows.

$$\begin{cases} \dot{x}_1 = x_2 \\ \dot{x}_2 = x_3 + d_1 \\ \dot{x}_3 = f + g u + d_2 \end{cases} \quad (100)$$

wherein the dynamic functions are defined as:

$$\begin{cases} f = \frac{\beta_e}{m} \left[\frac{A_1}{V_{1t}} (-A_1 + (A_1 - A_2) sm(-x_2)) - \frac{A_2}{V_{2t}} (A_2 + (A_1 - A_2) sm(x_2)) \right] x_2 \\ g = \frac{\beta_e \eta_V DK_{dr}}{m} \left(\frac{A_1}{V_{1t}} + \frac{A_2}{V_{2t}} \right) \\ d_1 = \frac{1}{m} (f_{Fr} + \delta_2) \\ d_2 = -\frac{\beta_e}{m} C_{Li} (P_1 - P_2) \left(\frac{A_1}{V_{1t}} + \frac{A_2}{V_{2t}} \right) + \frac{A_1 \delta_{31}}{m V_{1t}} - \frac{A_2 \delta_{32}}{m V_{2t}} \end{cases} \quad (101)$$

Parameter description can be found in Table 2. In (100), the disturbance d_1 exists in a different channel from the control input u , thus it is a mismatched disturbance. Whereas, the disturbance d_2 is a matched one. To estimate the mismatched disturbance d_1 , a finite-time disturbance observer can be designed based on (52) as follows.

$$\begin{cases} \dot{z}_{12} = v_{12} + x_3 \\ v_{12} = -\lambda_{12} L_2^{1/4} |z_{12} - x_2|^{3/4} \text{sign}(z_{12} - x_2) - \mu_{12} (z_{12} - x_2) + z_{22} \\ \dot{z}_{22} = v_{22} \\ v_{22} = -\lambda_{22} L_2^{1/3} |z_{22} - v_{12}|^{2/3} \text{sign}(z_{22} - v_{12}) - \mu_{22} (z_{22} - v_{12}) + z_{32} \\ \dot{z}_{32} = v_{32} \\ v_{32} = -\lambda_{32} L_2^{1/2} |z_{32} - v_{22}|^{1/2} \text{sign}(z_{32} - v_{22}) - \mu_{32} (z_{32} - v_{22}) + z_{42} \\ \dot{z}_{42} = -\lambda_{42} L_2 \text{sign}(z_{42} - v_{32}) - \mu_{42} (z_{42} - v_{32}) \end{cases} \quad (102)$$

where $z_{12} = \hat{x}_2$, $z_{22} = \hat{d}_1$, $z_{32} = \hat{d}_1$, $z_{42} = \hat{d}_1$, and $L_2 > 0$, $\lambda_{j2}, \mu_{j2} > 0$ ($j=1, \dots, 4$). Toward the problem of position tracking control, a chattering-free full-order TSMC surface can be then designed as below.

$$\sigma = \dot{e}_3 + c_3 |e_3 + z_{22}|^{\alpha_3} \text{sign}(e_3 + z_{22}) + c_2 |e_2|^{\alpha_2} \text{sign}(e_2) + c_1 |e_1|^{\alpha_1} \text{sign}(e_1) + z_{32} \quad (103)$$

where c_i ($i=1, 2, 3$) are positive constants satisfying the polynomial $p^3 + c_3 p^2 + c_2 p + c_1$ is Hurwitz; α_i ($i=1, 2, 3$) are chosen following (55) such that:

$$\begin{cases} \alpha_3 = \alpha, \alpha \in (1 - \varepsilon, 1), \varepsilon \in (0, 1) \\ \alpha_{k-1} = \frac{\alpha_k \alpha_{k+1}}{2\alpha_{k+1} - \alpha_k}, k = 2, 3 \end{cases} \quad (104)$$

Also, $e_1 = x_1 - r$, $e_2 = x_2 - \dot{r}$, $e_3 = x_3 - \ddot{r}$ are the system errors with r is the desired position trajectory. These above system errors establish the following equation set:

$$\begin{cases} \dot{e}_1 = e_2 \\ \dot{e}_2 = e_3 + d_1 \\ \dot{e}_3 = f - \ddot{r} + gu + d_2 \end{cases} \quad (105)$$

Based on the sliding surface (103), a control law is developed with the form of:

$$u = g^{-1}(u_{eq} + u_n) \quad (106)$$

where u_{eq} denotes the equivalent control signal and is defined as:

$$u_{eq} = -f + \ddot{r} - c_3 |e_3 + z_{22}|^{\alpha_3} \text{sign}(e_3 + z_{22}) - c_2 |e_2|^{\alpha_2} \text{sign}(e_2) - c_1 |e_1|^{\alpha_1} \text{sign}(e_1) - z_{32} \quad (107)$$

and the switching term u_n is designed and filtered as follows.

$$\begin{cases} \dot{u}_n + Tu_n = v \\ v = -(\rho_2 + k_T + \eta) \text{sign}(\sigma) \end{cases} \quad (108)$$

The nominal value of system parameters can be found in Table 3 in Section 4.2. The deviations of real system parameters from their nominal values can be added to the disturbances $d_{1,2}$.

The testing system consists of the studied model and a control data acquisition system. The system apparatus is shown in Figure 27. A load module was installed on the opposite side of the control system. Adjusting manually the cracking pressures of the relief valves can vary the loading condition. It is worth mentioning that the external load created by the opposite hydraulic system introduces highly nonlinear characteristics into the system. These nonlinear characteristics attribute to not only the displacement and velocity of the actuator but also to the cracking pressures of the loading relief valves as well as the different areas at the bore side and rod side of the cylinders. The control data acquisition system includes an Advantech Industrial Computer (Core i5-4570 3.2 GHz 4CPUs), a data acquisition card (PCI-6221), an encoder reader (PCI-QUAD 04) and a sensor system. Displacement of the actuator and working pressures of the system are recorded by a linear encoder (WTB5-500 MM) and pressure transducers (DS-230), respectively. The external force is measured using a load cell (YC60-2T) and an indicator. The designed controller is implemented in the computer using the real-time window target toolbox of MATLAB with a sampling time of 5ms.

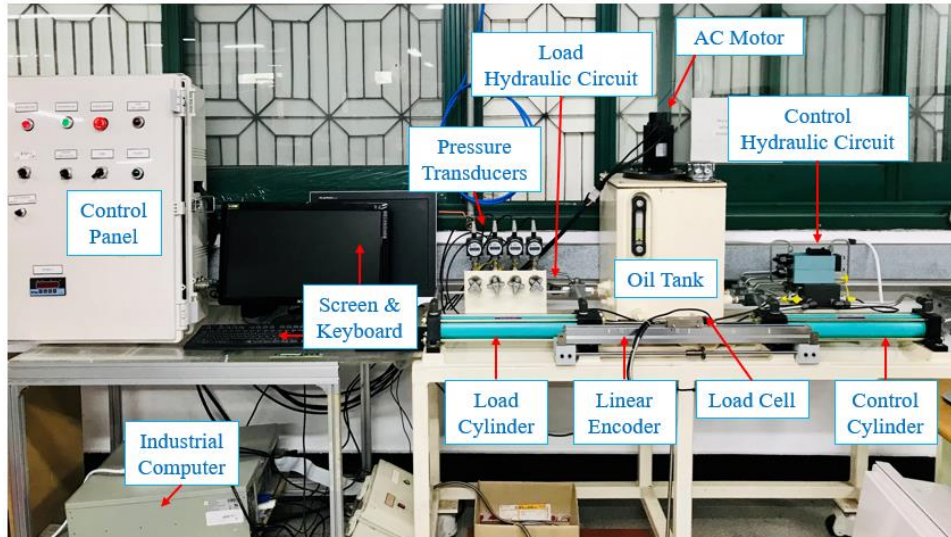


Figure 27. Photograph of the experimental apparatus.

The control gains and estimation gains are selected as follows. For the TSMC controller, $c_1 = 44$, $c_2 = 24$, $c_3 = 24$, $\alpha_1 = 1/3$, $\alpha_2 = 3/7$, $\alpha_3 = 3/5$, $T = 0.1$, and $\beta = (\rho_2 + k_T + \eta) = 144$.

For the disturbance observer, $L_2 = 500$, $\lambda_{12} = 12$, $\lambda_{22} = 9$, $\lambda_{32} = 6$, $\lambda_{42} = 3$, $\mu_{12} = 48$, $\mu_{22} = 44$, $\mu_{32} = 24$, $\mu_{42} = 12$.

To verify the effectiveness of the proposed control algorithm, the popular PID controller is selected for comparison purpose. The reason PID is chosen lies in the fact that PID is an effective error-based control algorithm and simple to interpret and implement. Thus, PID is commonly found in enormous applications. If being well-tuned, PID can provide relatively satisfactory results for the control system. In this experiment, the PID gains are manually tuned to be $K_P = 795$, $K_I = 270$, and $K_D = 30$ using the trial-and-error method.

The experiment is carried out with a reference input of a sinusoidal signal, $r = 50\sin(\pi t)$ mm . After applying the two control algorithms, the experimental results are plotted in Figure 28 to Figure 31.

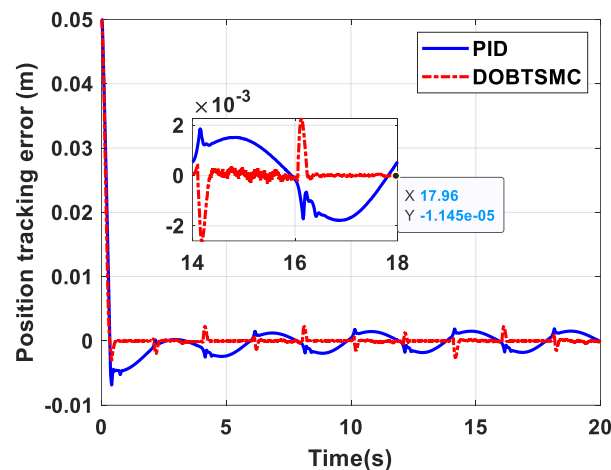


Figure 28. Position tracking errors of PID and the proposed controller.

Figure 28 illustrates the position tracking errors of PID and the proposed control algorithm on the target system. The error delivered by PID reaches and then varies in a small bounded region around the equilibrium without actually converging to it. Despite the high nonlinearity of the target system, PID can produce a relatively good control error in the range of $\pm 2\text{mm}$ ($\sim 4\%$). Even though the PID controller can achieve higher accuracy if higher gains are set, its position tracking error is expected to never converge to zero because PID is a linear type of controller. Also, large PID gains might drive the control performance to pass its limitations and the system stability might be vulnerable over a wide range of operations [52]. Whereas, much higher accuracy is seen for the proposed controller, $\pm 0.02\text{mm}$ ($\sim 0.04\%$). To achieve this result, the system mismatched disturbance is well observed and subsequently compensated

by the controller, which is shown in Figure 30. Abnormal surges are seen as the cylinder change its moving direction. This can be explained due to the mechanical failure of the structure and the lagging effects in the sensing system.

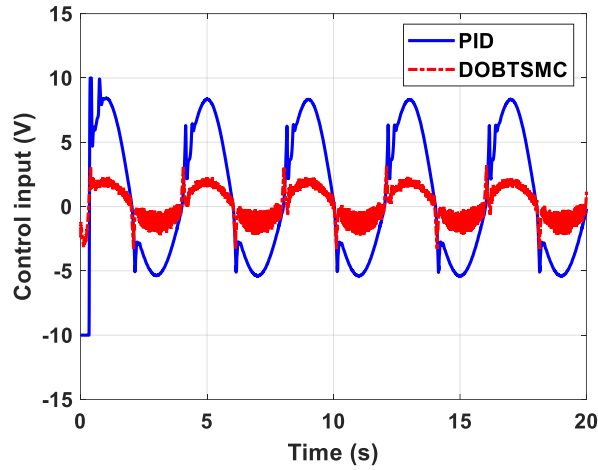


Figure 29. Control input trajectory of PID and the proposed control algorithm.

The control input trajectories of the two considered controllers are presented in Figure 29. It can be observed that smaller control efforts are seen in the proposed controller. However, the chattering phenomenon still exists in the proposed control signal, which indicates a shortcoming in practical applications.

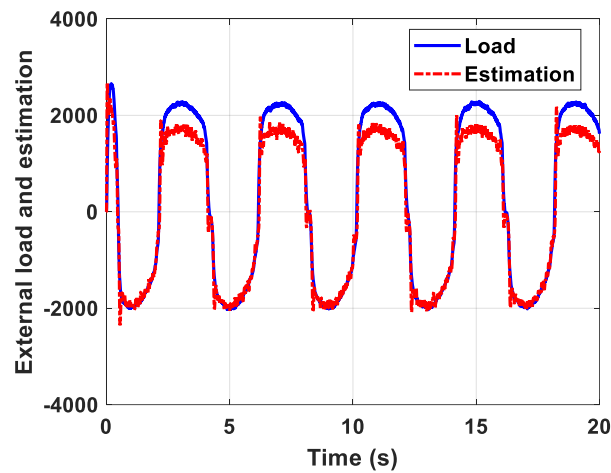


Figure 30. External force and its estimation using the proposed disturbance observer.

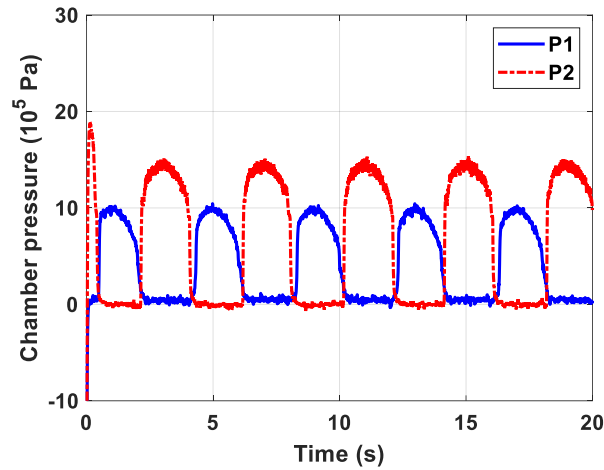


Figure 31. Working pressures of cylinder chambers.

Figure 30 demonstrates the performance of the proposed disturbance observer. The fact that there are failures at only one side of the external load trajectory might lie in the asymmetric structure of the single-rod cylinder, where the areas of the two chambers are different from each other. Figure 31 records the working pressure inside two chambers. The discrepancy in the area of the two chambers explains the difference in magnitude of the two pressure. Since $A_2 < A_1$, P_2 must be larger than P_1 to produce the same output force, for instance.

In this section, the effectiveness of the proposed controller was evaluated in dealing with the problem of position tracking control for an EHA system. The proposed control algorithm was compared with the PID controller, which is an error-based controller and widely found in the industry. Much higher precision in position tracking is achieved by the proposed controller owing to both the relatively accurate estimation of mismatched disturbance and the robustness of the sliding mode control. However, the proposed control algorithm still exhibits an undesired chattering phenomenon in its control signal, which might prevent it from being popular in practice.

CONCLUSION AND FUTURE WORK

5.1 Summary

This dissertation introduces a new control algorithm for a class of nonlinear systems subject to both matched and mismatched disturbances. To suppress the nonlinearity and to overcome the negative effects of disturbances on the system, a disturbance-observer-based chattering-free full-order terminal sliding mode control is proposed, developed and investigated. Mathematical modeling, controller design, stability analysis, simulation, and experiment are given to support and validate the effectiveness of the proposed control algorithm. The following conclusions are drawn from the work.

(1) The nonlinear finite-time disturbance observer is developed based on the research on globally convergent differentiators in the literature. Using the information of system states, the disturbance observer is expected to estimate the mismatched disturbance and its derivatives in finite time. A set of observer parameters needs to be tuned to reach the level of high accuracy. Generally, the greater the value of observer parameters, the faster convergence of estimation errors, yet the larger peaking phenomena at the beginning if the initial values of the system states and those of the observer are different. Thus, in the case of different initial values, a tradeoff should be made to ensure fast convergence yet acceptable peaking phenomena.

(2) The influences of nonlinear dynamics and matched disturbances are overcome by the robustness of a terminal sliding mode control design. To alleviate the chattering phenomenon, the switching control signal is defined and filtered in the same way as a low-pass filter. Also, the structure of full-order terminal sliding mode is employed so that the equivalent control signal can be derived without producing terms that could lead to singularity in some specific cases.

(3) Although the proposed control algorithm is first designed to address the problem of stabilization for a class of nonlinear second-order systems, it is then extended for the n th-order systems. Later, the proposed controller is also modified to tackle the problem of tracking control.

(4) Although in the studies, the proposed control has demonstrated its effectiveness in controlling different target systems, more rigorous studies should be carried out in future work for better evaluation. Specifically, in the task of controlling a bidirectional DC-DC converter,

the converter is control-oriented modeled so that it is more convenient to apply nonlinear control algorithms. However, this approach leads to a disadvantage as the virtual control signal is required to be large, subsequently, large control parameters are selected to produce such a control signal. Large control parameters make it more difficult for the tuning process. Whereas, in the study of position control for an electro hydrostatic actuator, although it is conducted in an experiment, different working scenarios should be added to the scheme. Also, the effect of the asymmetric cylinders on the system performance should be carefully studied.

5.2 Future work

(1) Throughout the study, the system states were assumed to be available to be collected. However, there are various cases in practice where only one system state such as displacement is available. Thus, one of the future works could focus on developing a high-performance finite-time extended-state disturbance observer to estimate both disturbances and remaining states of the system. Thus, more effectively control can be achieved.

(2) To carefully evaluate the effectiveness of the proposed control algorithm in solving the problem of controlling the bidirectional DC-DC converter, it should be tested in different working modes. These scenarios might include buck-boost switching or load changes. Also, not only simulations but also experiments should be conducted for better assessment.

References

- [1] D. Ginoya, P. D. Shendge, and S. B. Phadke, "Disturbance observer based sliding mode control of nonlinear mismatched uncertain systems," *Communications in Nonlinear Science and Numerical Simulation*, vol. 26, no. 1, pp. 98-107, 2015/09/01/ 2015, doi: <https://doi.org/10.1016/j.cnsns.2015.02.008>.
- [2] C. Jing, H. Xu, and X. Niu, "Adaptive sliding mode disturbance rejection control with prescribed performance for robotic manipulators," *ISA Transactions*, 2019/02/04/ 2019, doi: <https://doi.org/10.1016/j.isatra.2019.01.017>.
- [3] R. Mohammadi Asl, Y. Shabbouei Hagh, and R. Palm, "Robust control by adaptive Non-singular Terminal Sliding Mode," *Engineering Applications of Artificial Intelligence*, vol. 59, pp. 205-217, 2017/03/01/ 2017, doi: <https://doi.org/10.1016/j.engappai.2017.01.005>.
- [4] M.-D. Tran and H.-J. Kang, "Adaptive terminal sliding mode control of uncertain robotic manipulators based on local approximation of a dynamic system," *Neurocomputing*, vol. 228, pp. 231-240, 2017/03/08/ 2017, doi: <https://doi.org/10.1016/j.neucom.2016.09.089>.
- [5] Y. Zhao, Y. Zhang, and J. Lee, "Lyapunov and sliding mode based leader-follower formation control for multiple mobile robots with an augmented distance-angle strategy," *International Journal of Control, Automation and Systems*, vol. 17, no. 5, pp. 1314-1321, 2019.
- [6] Z. Jin, Z. Liang, X. Wang, and M. Zheng, "Adaptive Backstepping Sliding Mode Control of Tractor-trailer System with Input Delay Based on RBF Neural Network," *International Journal of Control, Automation and Systems*, vol. 19, no. 1, pp. 76-87, 2021.
- [7] D. Jiang, W. Yu, J. Wang, Y. Zhao, Y. Li, and Y. Lu, "A Speed Disturbance Control Method Based on Sliding Mode Control of Permanent Magnet Synchronous Linear Motor," *IEEE Access*, vol. 7, pp. 82424-82433, 2019, doi: 10.1109/ACCESS.2019.2922765.
- [8] Y. Gao, Y. Wu, X. Wang, and Q. Chen, "Characteristic model-based adaptive control with genetic algorithm estimators for four-pmsm synchronization system," *International Journal of Control, Automation and Systems*, pp. 1-12, 2020.

- [9] J. Wang, L. Zhao, and L. Yu, "Reduced-order Generalized Proportional Integral Observer Based Continuous Dynamic Sliding Mode Control for Magnetic Levitation System with Time-varying Disturbances," *International Journal of Control, Automation and Systems*, vol. 19, no. 1, pp. 439-448, 2021.
- [10] S. U. Din, Q. Khan, F. U. Rehman, and R. Akmeliawanti, "A Comparative Experimental Study of Robust Sliding Mode Control Strategies for Underactuated Systems," *IEEE Access*, vol. 6, pp. 1927-1939, 2018, doi: 10.1109/ACCESS.2017.2780889.
- [11] S. Mobayen, "An adaptive chattering-free PID sliding mode control based on dynamic sliding manifolds for a class of uncertain nonlinear systems," *Nonlinear Dynamics*, journal article vol. 82, no. 1, pp. 53-60, October 01 2015, doi: 10.1007/s11071-015-2137-7.
- [12] X. Zhang, L. Sun, K. Zhao, and L. Sun, "Nonlinear Speed Control for PMSM System Using Sliding-Mode Control and Disturbance Compensation Techniques," *IEEE Transactions on Power Electronics*, vol. 28, no. 3, pp. 1358-1365, 2013, doi: 10.1109/TPEL.2012.2206610.
- [13] Z. Chen, X. Tu, L. Xing, J. Fu, and R. Lozano, "A Special Kind of Sliding Mode Control for Nonlinear System With State Constraints," *IEEE Access*, vol. 7, pp. 69998-70010, 2019, doi: 10.1109/ACCESS.2019.2918786.
- [14] M. Kamalesh, N. Senthilnathan, and C. Bharatiraja, "Design of a Novel Boomerang Trajectory for Sliding Mode Controller," *International Journal of Control, Automation and Systems*, vol. 18, pp. 2917-2928, 2020.
- [15] D. Ye, H. Zhang, Y. Tian, Y. Zhao, and Z. Sun, "Fuzzy sliding mode control of nonparallel-ground-track imaging satellite with high precision," *International Journal of Control, Automation and Systems*, pp. 1-12, 2020.
- [16] S. S. Xu, C. Chen, and Z. Wu, "Study of Nonsingular Fast Terminal Sliding-Mode Fault-Tolerant Control," *IEEE Transactions on Industrial Electronics*, vol. 62, no. 6, pp. 3906-3913, 2015, doi: 10.1109/TIE.2015.2399397.
- [17] Y. Feng, M. Zhou, X. Zheng, F. Han, and X. Yu, "Full-order terminal sliding-mode control of MIMO systems with unmatched uncertainties," *Journal of the Franklin Institute*, vol. 355, no. 2, pp. 653-674, 2018/01/01/ 2018, doi: <https://doi.org/10.1016/j.jfranklin.2017.10.034>.

- [18] A. Levant, "Chattering Analysis," *IEEE Transactions on Automatic Control*, vol. 55, no. 6, pp. 1380-1389, 2010, doi: 10.1109/TAC.2010.2041973.
- [19] P. Kachroo and M. Tomizuka, "Chattering reduction and error convergence in the sliding-mode control of a class of nonlinear systems," *IEEE Transactions on Automatic Control*, vol. 41, no. 7, pp. 1063-1068, 1996, doi: 10.1109/9.508917.
- [20] G. Bartolini, A. Ferrara, and E. Usai, "Chattering avoidance by second-order sliding mode control," *IEEE Transactions on Automatic Control*, vol. 43, no. 2, pp. 241-246, 1998, doi: 10.1109/9.661074.
- [21] A. Levant, "Higher-order sliding modes, differentiation and output-feedback control," *International Journal of Control*, vol. 76, no. 9-10, pp. 924-941, 2003/01/01 2003, doi: 10.1080/0020717031000099029.
- [22] A. Levant, "Principles of 2-sliding mode design," *Automatica*, vol. 43, no. 4, pp. 576-586, 2007/04/01/ 2007, doi: <https://doi.org/10.1016/j.automatica.2006.10.008>.
- [23] X. Jian-Xin, P. Ya-Jun, and L. Tong-Heng, "Sliding mode control with closed-loop filtering architecture for a class of nonlinear systems," *IEEE Transactions on Circuits and Systems II: Express Briefs*, vol. 51, no. 4, pp. 168-173, 2004, doi: 10.1109/TCSII.2004.824066.
- [24] M.-L. Tseng and M.-S. Chen, "Chattering reduction of sliding mode control by low-pass filtering the control signal," *Asian Journal of Control*, vol. 12, no. 3, pp. 392-398, 2010, doi: 10.1002/asjc.195.
- [25] A. Kawamura, H. Itoh, and K. Sakamoto, "Chattering reduction of disturbance observer based sliding mode control," *IEEE Transactions on Industry Applications*, vol. 30, no. 2, pp. 456-461, 1994, doi: 10.1109/28.287509.
- [26] C. Mu and H. He, "Dynamic Behavior of Terminal Sliding Mode Control," *IEEE Transactions on Industrial Electronics*, vol. 65, no. 4, pp. 3480-3490, 2018, doi: 10.1109/TIE.2017.2764842.
- [27] M. L. Corradini and A. Cristofaro, "Nonsingular terminal sliding-mode control of nonlinear planar systems with global fixed-time stability guarantees," *Automatica*, vol. 95, pp. 561-565, 2018/09/01/ 2018, doi: <https://doi.org/10.1016/j.automatica.2018.06.032>.
- [28] H. Rabiee, M. Ataei, and M. Ekramian, "Continuous nonsingular terminal sliding mode control based on adaptive sliding mode disturbance observer for uncertain nonlinear

- systems," *Automatica*, vol. 109, p. 108515, 2019/11/01/ 2019, doi: <https://doi.org/10.1016/j.automatica.2019.108515>.
- [29] Y. Wang, K. Zhu, F. Yan, and B. Chen, "Adaptive super-twisting nonsingular fast terminal sliding mode control for cable-driven manipulators using time-delay estimation," *Advances in Engineering Software*, vol. 128, pp. 113-124, 2019/02/01/ 2019, doi: <https://doi.org/10.1016/j.advengsoft.2018.11.006>.
- [30] Y. Feng, F. Han, and X. Yu, "Chattering free full-order sliding-mode control," *Automatica*, vol. 50, no. 4, pp. 1310-1314, 2014/04/01/ 2014, doi: <https://doi.org/10.1016/j.automatica.2014.01.004>.
- [31] J. Wang, S. Li, J. Yang, B. Wu, and Q. Li, "Finite-time disturbance observer based non-singular terminal sliding-mode control for pulse width modulation based DC–DC buck converters with mismatched load disturbances," *IET Power Electronics*, vol. 9, no. 9, pp. 1995-2002. [Online]. Available: <https://digital-library.theiet.org/content/journals/10.1049/iet-pel.2015.0178>
- [32] V. Utkin and S. Jingxin, "Integral sliding mode in systems operating under uncertainty conditions," in *Proceedings of 35th IEEE Conference on Decision and Control*, 13-13 Dec. 1996 1996, vol. 4, pp. 4591-4596 vol.4, doi: 10.1109/CDC.1996.577594. [Online]. Available: <https://ieeexplore.ieee.org/ielx3/4303/12517/00577594.pdf?tp=&arnumber=577594&inumber=12517&ref=>
- [33] C. Wen-Jun and X. Jian-Xin, "Nonlinear integral-type sliding surface for both matched and unmatched uncertain systems," *IEEE Transactions on Automatic Control*, vol. 49, no. 8, pp. 1355-1360, 2004, doi: 10.1109/TAC.2004.832658.
- [34] F. Castanos and L. Fridman, "Analysis and design of integral sliding manifolds for systems with unmatched perturbations," *IEEE Transactions on Automatic Control*, vol. 51, no. 5, pp. 853-858, 2006, doi: 10.1109/TAC.2006.875008.
- [35] S. Mondal and C. Mahanta, "Chattering free adaptive multivariable sliding mode controller for systems with matched and mismatched uncertainty," *ISA Transactions*, vol. 52, no. 3, pp. 335-341, 2013/05/01/ 2013, doi: <https://doi.org/10.1016/j.isatra.2012.12.007>.
- [36] C.-M. Kwan, "Sliding mode control of linear systems with mismatched uncertainties," *Automatica*, vol. 31, no. 2, pp. 303-307, 1995/02/01/ 1995, doi: [https://doi.org/10.1016/0005-1098\(94\)00093-X](https://doi.org/10.1016/0005-1098(94)00093-X).

- [37] C.-C. Wen and C.-C. Cheng, "Design of sliding surface for mismatched uncertain systems to achieve asymptotical stability," *Journal of the Franklin Institute*, vol. 345, no. 8, pp. 926-941, 2008/11/01/ 2008, doi: <https://doi.org/10.1016/j.jfranklin.2008.06.003>.
- [38] J. Yang, S. Li, and X. Yu, "Sliding-Mode Control for Systems With Mismatched Uncertainties via a Disturbance Observer," *IEEE Transactions on Industrial Electronics*, vol. 60, no. 1, pp. 160-169, 2013, doi: 10.1109/TIE.2012.2183841.
- [39] D. Ginoya, P. D. Shendge, and S. B. Phadke, "Sliding Mode Control for Mismatched Uncertain Systems Using an Extended Disturbance Observer," *IEEE Transactions on Industrial Electronics*, vol. 61, no. 4, pp. 1983-1992, 2014, doi: 10.1109/TIE.2013.2271597.
- [40] J. Zhang, X. Liu, Y. Xia, Z. Zuo, and Y. Wang, "Disturbance Observer-Based Integral Sliding-Mode Control for Systems With Mismatched Disturbances," *IEEE Transactions on Industrial Electronics*, vol. 63, no. 11, pp. 7040-7048, 2016, doi: 10.1109/TIE.2016.2583999.
- [41] S. Shi, J. Li, and Y. Fang, "Extended-State-Observer-Based Chattering Free Sliding Mode Control for Nonlinear Systems With Mismatched Disturbance," *IEEE Access*, vol. 6, pp. 22952-22957, 2018, doi: 10.1109/ACCESS.2018.2828868.
- [42] N. P. Nguyen, H. Oh, Y. Kim, and J. Moon, "Disturbance Observer-Based Continuous Finite-Time Sliding Mode Control against Matched and Mismatched Disturbances," *Complexity*, vol. 2020, 2020.
- [43] W.-H. Chen, "Nonlinear disturbance observer-enhanced dynamic inversion control of missiles," *Journal of Guidance, Control, and Dynamics*, vol. 26, no. 1, pp. 161-166, 2003.
- [44] J. Su, J. Yang, and S. Li, "Continuous finite-time anti-disturbance control for a class of uncertain nonlinear system," *Transactions of the Institute of Measurement and Control*, 05/06 2013, doi: 10.1177/0142331213499182.
- [45] J. Yang, S. Li, J. Su, and X. Yu, "Continuous nonsingular terminal sliding mode control for systems with mismatched disturbances," *Automatica*, vol. 49, no. 7, pp. 2287-2291, 2013/07/01/ 2013, doi: <https://doi.org/10.1016/j.automatica.2013.03.026>.
- [46] J. Yang, J. Su, S. Li, and X. Yu, "High-Order Mismatched Disturbance Compensation for Motion Control Systems Via a Continuous Dynamic Sliding-Mode Approach,"

- IEEE Transactions on Industrial Informatics*, vol. 10, no. 1, pp. 604-614, 2014, doi: 10.1109/TII.2013.2279232.
- [47] S. P. Bhat and D. S. Bernstein, "Geometric homogeneity with applications to finite-time stability," *Mathematics of Control, Signals and Systems*, journal article vol. 17, no. 2, pp. 101-127, June 01 2005, doi: 10.1007/s00498-005-0151-x.
- [48] Y. Feng, F. Han, and X. Yu, "Reply to ‘Comments on ‘Chattering free full-order sliding-mode control’ [Automatica 50 (2014) 1310–1314]’," *Automatica*, vol. 72, pp. 255-256, 2016/10/01/ 2016, doi: <https://doi.org/10.1016/j.automatica.2016.04.036>.
- [49] S. P. Bhat and D. S. Bernstein, "Finite-time stability of homogeneous systems," in *Proceedings of the 1997 American Control Conference (Cat. No.97CH36041)*, 6-6 June 1997 1997, vol. 4, pp. 2513-2514 vol.4, doi: 10.1109/ACC.1997.609245. [Online]. Available: <https://ieeexplore.ieee.org/ielx3/4827/13338/00609245.pdf?tp=&arnumber=609245&inumber=13338&ref=>
- [50] A. Levant and M. Livne, "Globally convergent differentiators with variable gains," *International Journal of Control*, vol. 91, no. 9, pp. 1994-2008, 2018.
- [51] A. Levant, "Homogeneity approach to high-order sliding mode design," *Automatica*, vol. 41, no. 5, pp. 823-830, 2005/05/01/ 2005, doi: <https://doi.org/10.1016/j.automatica.2004.11.029>.
- [52] D. X. Ba, T. Q. Dinh, J. Bae, and K. K. Ahn, "An Effective Disturbance-Observer-Based Nonlinear Controller for a Pump-Controlled Hydraulic System," *IEEE/ASME Transactions on Mechatronics*, vol. 25, no. 1, pp. 32-43, 2020, doi: 10.1109/TMECH.2019.2946871.
- [53] J. Yao, Z. Jiao, D. Ma, and L. Yan, "High-Accuracy Tracking Control of Hydraulic Rotary Actuators With Modeling Uncertainties," *IEEE/ASME Transactions on Mechatronics*, vol. 19, no. 2, pp. 633-641, 2014, doi: 10.1109/TMECH.2013.2252360.
- [54] D. Won, W. Kim, D. Shin, and C. C. Chung, "High-Gain Disturbance Observer-Based Backstepping Control With Output Tracking Error Constraint for Electro-Hydraulic Systems," *IEEE Transactions on Control Systems Technology*, vol. 23, no. 2, pp. 787-795, 2015, doi: 10.1109/TCST.2014.2325895.
- [55] H. E. Merritt and V. Pomper, "Hydraulic control systems," *Journal of Applied Mechanics*, vol. 35, no. 1, p. 200, 1968.

- [56] D. X. Ba, K. K. Ahn, D. Q. Truong, and H. G. Park, "Integrated model-based backstepping control for an electro-hydraulic system," *International Journal of Precision Engineering and Manufacturing*, journal article vol. 17, no. 5, pp. 565-577, May 01 2016, doi: 10.1007/s12541-016-0069-x.
- [57] J. Zhang, "Bidirectional DC-DC power converter design optimization, modeling and control," Virginia Tech, 2008.